



HAL
open science

Lobe dynamics in a kinematic model of a meandering jet. I. Geometry and statistics of transport and lobe dynamics with accelerated convergence

Florence Raynal, S. Wiggins

► **To cite this version:**

Florence Raynal, S. Wiggins. Lobe dynamics in a kinematic model of a meandering jet. I. Geometry and statistics of transport and lobe dynamics with accelerated convergence. *Physica D: Nonlinear Phenomena*, 2006, 223, pp.7-25. 10.1016/j.physd.2006.07.021 . hal-00274861

HAL Id: hal-00274861

<https://hal.science/hal-00274861>

Submitted on 20 Jul 2016

HAL is a multi-disciplinary open access archive for the deposit and dissemination of scientific research documents, whether they are published or not. The documents may come from teaching and research institutions in France or abroad, or from public or private research centers.

L'archive ouverte pluridisciplinaire **HAL**, est destinée au dépôt et à la diffusion de documents scientifiques de niveau recherche, publiés ou non, émanant des établissements d'enseignement et de recherche français ou étrangers, des laboratoires publics ou privés.

Lobe Dynamics in a Kinematic Model of a Meandering Jet, I: Geometry and Statistics of Transport and Lobe Dynamics with Accelerated Convergence

Florence Raynal
Laboratoire de Mécanique des Fluides et d'Acoustique
UMR CNRS 5509
École Centrale de Lyon et Université Claude Bernard Lyon I
36 avenue de Collongue
69 134 Ecully
France

Stephen Wiggins *
School of Mathematics
University of Bristol
University Walk
Bristol, BS8 1TW
United Kingdom

April 21, 2006

Abstract

In geophysical fluid mechanics a meandering jet is a fundamental flow structure arising in a variety of diverse settings. In this paper we apply the method of lobe dynamics to study transport associated with a kinematic model of a meandering jet. We describe in detail the geometric structure of cross jet transport. In particular, we describe the mechanisms for particles to cross the jet, to enter the jet from a certain region and to leave it by exiting into the same region, and to escape from the jet, all in terms of lobe dynamics. Furthermore, we are able to derive a number of statistical quantities in terms of lobe dynamics, such as the average time to cross the jet for particles entering the jet and the average residence time for particles in the jet. These statistical quantities are expressed in terms of infinite series of areas of intersections of turnstile lobes. We develop a procedure for achieving “accelerated convergence” of these series which yields a good approximation to the exact result with a low order truncation of the series.

*This research was supported by ONR Grant No. N00014-01-1-0769.

1 Introduction

In this paper we will be concerned with fluid parcel motions in kinematical models of meandering jets. This has been a subject attracting much attention in recent years, largely motivated by the work of Bower [1991]. Based on RAFOS float observations of the Gulf Stream, she devised a kinematical model consisting of a jet of uniform width deformed by a steadily propagating sinusoidal meander. In a reference frame moving with the meander the fluid motion is steady and, for eastward meander propagation, consisted of three regimes; a central jet, exterior retrograde motion, and intermediate closed circulations above meander troughs and below crests. Since the fluid motion was steady no exchange could occur between the three regimes. However, float observations indicate that exchange does occur across some parts of the Gulf stream. Samelson [1992] recognized that this must be due to deviations from the regular pattern of Bower’s model and modified her model to include additional spatio-temporal variability in the velocity field. In particular, he allowed for a time-dependent meander amplitude, a time-dependent spatially uniform meridional velocity superimposed on the basic flow, and a propagating plane wave superimposed on the basic flow.

Samelson’s work was also significant in that it showed the usefulness in oceanography of dynamical systems techniques for the study of Lagrangian transport. In particular, the boundaries of the different flow regimes associated with the jet are made up of stable and unstable manifolds of hyperbolic trajectories. If the temporal variability is periodic or quasiperiodic, then chaotic fluid particle trajectories can be inferred from the transversal intersection of the stable and unstable manifolds of a hyperbolic trajectory. Flux between the different regions can also be computed in the case where the temporal variability is “small” by using the Melnikov function. Further analysis of kinematic models can be found in Boffetta *et al.* [2001] and Duan and Wiggins [1996]. The work on kinematic models paved the way for similar studies on more physically realistic dynamically consistent models. See Rogerson *et al.* [1999], Poje and Haller [1999], and Yuan *et al.* [2002]. A recent review of this problem, as well as a review of applying dynamical systems ideas to study transport in oceanic flows in general, can be found in Wiggins [2005].

However, none of these studies have brought to bear the full power of the dynamical systems based transport methods on the meandering jet. The studies thus far have been limited to a study of exchange between adjacent flow regimes and an inference of chaotic parcel trajectories based on the Smale-Birkhoff theorem. Strictly speaking, the construction of the chaotic invariant set in the Smale-Birkhoff theorem is done on an arbitrarily small region of the flow, although afterwards some effort is usually made to indicate how this could plausibly occur in more global regions of the flow.

In this paper we give a detailed study of transport associated with the meandering jet using the technique of *lobe dynamics* as described in Rom-Kedar and Wiggins [1990] and Rom-Kedar [1994]. In Part II we show how lobe dynamics can be used to construct *global* horseshoes and relate the chaotic motion of the horseshoes to specific types of particle trajectories. Our analysis provides a detailed understanding of global chaos associated with this model on both finite and infinite time scales. Moreover, it provides estimates for the stretching rates of fluid line elements as well as upper and lower bounds on Lyapunov exponents.

This paper is organized as follows. In Section 2 we describe the kinematic model of the meandering jet due to Bower and Samelson. In particular, we describe the five distinct regions of the flow separated by stable and unstable manifolds of hyperbolic trajectories. Section 3 is concerned with the analysis of transport based on lobe dynamics. We begin by describing the turnstile mechanism. Turnstile lobe dynamics are then used to describe in detail the geometry associated with particles entering the jet from the north. In particular, we describe how particles can cross the jet and exit to the south, as well as exit the jet back to the north. We also develop several statistical measures to quantify transport associated with the jet. We derive an expression for the average time to cross the jet for particles entering the jet from the north solely in terms of turnstile lobe dynamics. We derive similar statistical quantities for particles that enter the jet from the north and exit the jet back to the north at some later time without crossing the jet. [The statistical quantities are expressed in terms of infinite series of areas of intersections of turnstile lobes.](#) We then derive geometrical constraints on those series, which give rise to an expression for the mean residence time in the jet, and finally study the escape rate from the jet. All the results in this section can be considered as exact results from lobe dynamics. In section 4 we show essentially numerical results: we introduce the four sets of parameters chosen for this study, and then present exit time statistics and escape rate from the central region R_3 . In particular we show that the statistics for fluid leaving by the south or the north are rather proportional; this is explained in terms of [well-mixed hypothesis](#). Then in section 5 we show how to use both the well-mixed hypothesis and

low order truncation of the infinite series in order to derive *mixed series* that converge much faster so that a low order truncation gives a good answer. This allows to calculate statistics of mean crossing times using only a finite piece of manifolds, so that this method can be used for a real-data problem. We finally verify our results for the sets of parameters chosen, with good agreement.

2 The Kinematic Model of the Meandering Jet

We briefly describe the model of the meandering jet studied by Bower [1991] and Samelson [1992], and we follow the notation of this latter reference as closely as possible.

The streamfunction for the basic meandering jet has the form

$$\psi(x', y, t) = \psi_0 \left[1 - \tanh \left(\frac{y - A \cos k(x' - c_x t)}{\lambda (1 + k^2 A^2 \sin^2 k(x' - c_x t))^{\frac{1}{2}}} \right) \right], \quad (1)$$

where x' and y are cartesian coordinates indicating positive eastward and northward, respectively, $2\psi_0$ is referred to as the total eastward transport, λ determines the width of the jet, and A , k , and c_x are, respectively, the amplitude, wavenumber, and phase speed of the meander. A frame of reference moving with the meander is given by

$$X = x' - c_x t, \quad Y = y, \quad (2)$$

and in this frame the streamfunction, after nondimensionalization, takes the form

$$\phi(\xi, \eta) = 1 - \tanh \left[\frac{\eta - B \cos \kappa \xi}{(1 + \kappa^2 B^2 \sin^2 \kappa \xi)^{\frac{1}{2}}} \right] + c\eta, \quad (3)$$

where

$$\phi = \psi_0^{-1} \psi + c\eta, \quad (\xi, \eta) = \lambda^{-1} (X, Y), \quad B = \lambda^{-1} A,$$

$$\kappa = 2\pi L^{-1} = k\lambda, \quad c = \lambda \psi_0^{-1} c_x,$$

and the dimensionless time and length are given by

$$\tau = \psi_0 \lambda^{-2} t, \quad x = \lambda^{-1} x'.$$

2.1 Streamlines of the Steady Flow

Following Samelson [1992], we will fix the parameters for the basic meandering jet at the following values:

$$B = 1.2, \quad L = \frac{2\pi}{\kappa} = 10, .$$

c is varied in between 0.1 and 0.2.

In Fig.1 we sketch only the separatrices associated with the jet in the moving frame, and we see that there are three distinct types of fluid parcel trajectories— eastward moving parcels in the jet, westward moving parcels exterior to the jet, and parcels that execute periodic trajectories. These three types of trajectories exist in five distinct regions whose boundaries consist of separatrices connecting saddle-type stagnation points. In the figure the regions bounded by the separatrices are denoted by R_i , $i = 1, \dots, 5$. Since the flow is steady in the moving frame no exchange between these regions can occur in the moving frame. Hence, no transport of fluid parcels into or out of the jet can occur in the moving frame.

2.2 Temporal Variability

Samelson [1992] considers three types of variability in the moving frame; a periodically varying meander amplitude, a superimposed periodically time varying spatially uniform meridional flow, and a superimposed propagating wavetrain. We will only consider these first two types of variability in this paper: a periodically varying meander amplitude of the form:

$$B = B(t) = B_0(1 + \epsilon_1 \cos \omega t), \quad (4)$$

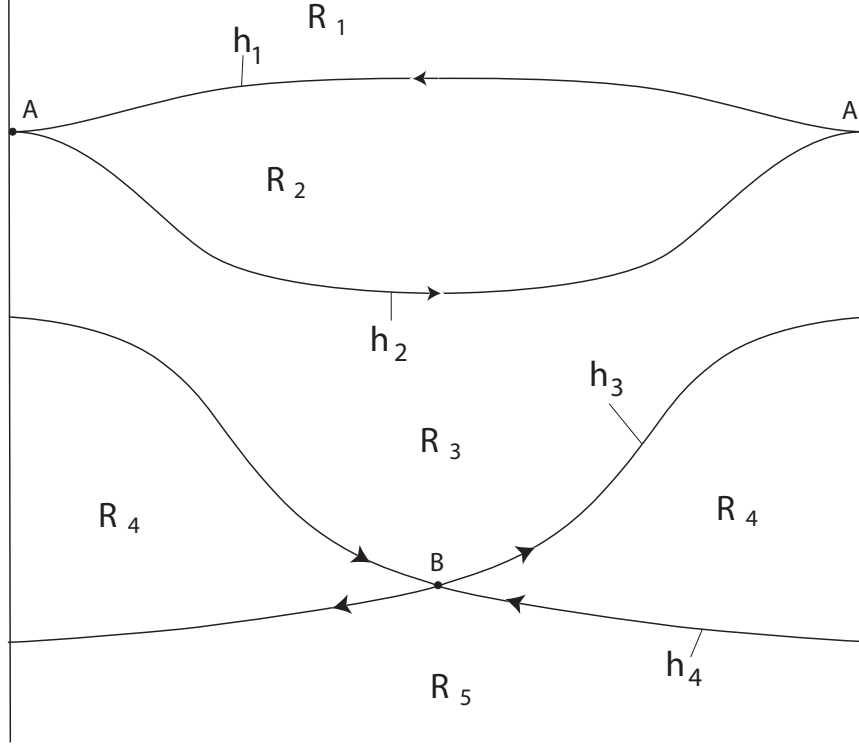


Figure 1: The different regions of the flow in the unperturbed jet. The points A and B denote saddle-type (hyperbolic) stagnation points. They are connected by streamlines h_1 , h_2 , h_3 , and h_4 that divide the flow into five qualitatively distinct regions. A region of northern retrograde particle trajectories, R_1 . The northern region of recirculating particles, R_2 . The jet, R_3 . The southern region of recirculating particles, R_4 . A region of southern retrograde particle trajectories, R_5 . The flow is periodic in the horizontal variable, ξ , with period $\frac{2\pi}{\kappa}$. We are illustrating one period in ξ .

and the superimposed periodically time varying spatially uniform meridional flow:

$$\phi(\xi, \eta, t) = \phi_1(\xi, \eta, t) - \epsilon_2 \xi \sin(\omega t), \quad (5)$$

where $\phi_1(\xi, \eta, t)$ is the streamfunction (3) with variability given by (4) alone.

The fluid particle trajectories are therefore given by :

$$\begin{aligned}\frac{d\xi}{dt} &= -c + \frac{1}{\sqrt{1 + B^2(t)\kappa^2 \sin^2(\kappa\xi)}} \sec\left(\frac{\eta - B(t)\cos(\kappa\xi)}{\sqrt{1 + B^2(t)\kappa^2 \sin^2(\kappa\xi)}}\right) \\ \frac{d\eta}{dt} &= -\sin(\kappa\xi) \frac{B(t)\kappa + B^2(t)\kappa^3(B(t) - \eta\cos(\kappa\xi))}{(1 + B^2(t)\kappa^2 \sin^2(\kappa\xi))^{3/2}} \sec\left(\frac{\eta - B(t)\cos(\kappa\xi)}{\sqrt{1 + B^2(t)\kappa^2 \sin^2(\kappa\xi)}}\right) + \epsilon_2 \sin(\omega t)\end{aligned}\quad (6)$$

In studying the particle trajectories of a time-periodic flow often one studies the associated Poincaré map. That is, rather than plotting trajectories as a function of time we plot their location at discrete intervals of time, where the interval of time is the period of the variability $T = \frac{2\pi}{\omega}$. More precisely, if $(\xi(t), \eta(t))$ is an arbitrary fluid particle trajectory then the associated Poincaré map, which we will denote by f , is given by:

$$f : (\xi(t_0), \eta(t_0)) \mapsto (\xi(t_0 + T), \eta(t_0 + T)). \quad (7)$$

In other words, at a fixed initial time t_0 , points are mapped to their location after flowing along a trajectory for one period.

The dynamics of two dimensional Poincaré maps have been studied thoroughly and (at least for ϵ somewhat small) we expect variability to “break up” the trajectories connected to the hyperbolic stagnation points shown in Fig. 1 and give rise to a complicated network of *homoclinic tangles* that we illustrate schematically in Fig. 2.

More precisely, for sufficiently small ϵ_1 and/or ϵ_2 (which, in practice could be rather large) the hyperbolic stagnation points become hyperbolic periodic trajectories, which are manifested as hyperbolic fixed points for the Poincaré map. These hyperbolic fixed points of the Poincaré map have one dimensional stable and unstable manifolds. These are *invariant curves* for the Poincaré map, i.e., trajectories that start on these curves always stay on these curves throughout the course of their time evolution (both in the future and the past). The fact that the curves are invariant means that they can act as *barriers to transport*. In fact, we will show that they form a geometrical template in space which constrains the temporal evolution of trajectories.

Finally, the existence of certain symmetries in the equations for fluid particle motions will be an important consideration when considering transport issues associated with the meandering jet. It is straightforward to verify that the equations for fluid particle motions (6) are unchanged after the following transformation:

$$\begin{aligned}t &\longrightarrow -t, \\ \xi &\longrightarrow L - \xi, \\ \eta &\longrightarrow \eta.\end{aligned}\quad (8)$$

For the Poincaré map this implies that the stable and unstable manifolds at $t_0 = 0$ are symmetric with respect to $x = L/2$. In addition, if $\epsilon_2 = 0$ (6) are unchanged after the following transformation:

$$\begin{aligned}t &\longrightarrow t, \\ \xi &\longrightarrow \frac{L}{2} + \xi, \\ \eta &\longrightarrow -\eta.\end{aligned}\quad (9)$$

The symmetry (9) is important. It implies that “north to south” transport is the same as “south to north” transport. Hence, we can break this symmetry by choosing $\epsilon_2 \neq 0$. This will play a role in our later analysis and discussions.

In the next three sections we will develop this theory. However, there is a very important point that should be grasped at this point. In the theoretical sections we will *assume* that a particular geometric relationship holds amongst the intersecting stable and unstable manifolds of the hyperbolic points of the Poincaré map. Then we will derive the consequences for transport from this geometric assumption. In order to verify that our results on transport are valid for the kinematic model of the meandering jet described above, we will

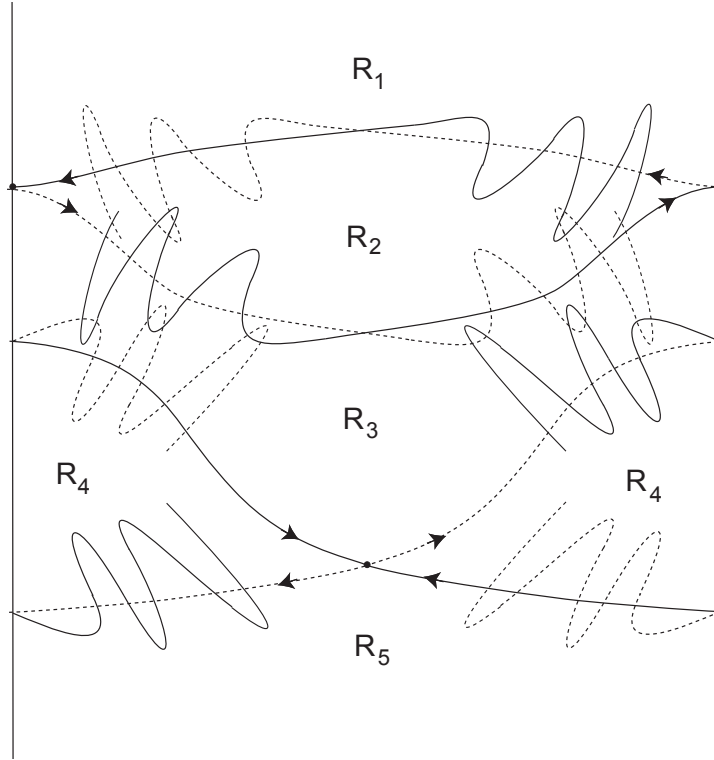


Figure 2: An illustration of a possible “homoclinic tangle” that may occur when variability is added to the steady jet in the moving frame.

have to perform a numerical validation that the necessary geometrical conditions on intersections of stable and unstable manifolds occur in the model. This we will address in the last section. However, it is important to realize that this illustrates the power of the dynamical systems approach for transport studies of this type. In particular, the details of the particular flow field are not so important. Rather, we only need to verify that certain geometrical criteria are satisfied in the flow. Consequently, our approach is not limited to kinematic models or to particular forms of the variability.

3 Lobe Dynamics and Transport for the Meandering Jet

In the unsteady (time-periodic) case we can use segments of the unstable manifolds of the hyperbolic trajectories to define regions analogous to those in the steady case. To do this we take segments of the stable and unstable manifolds that begin at hyperbolic points and end at chosen intersection points (the so-called *boundary intersection points*). This is shown in Fig. 3.

Because the domain is periodic on the horizontal coordinate, there are two distinct types of KAM tori that are possible. One is a KAM torus that is represented as a graph over the horizontal domain. Such a KAM torus completely encircles the domain and acts as a barrier separating fluid “below” and “above” the KAM torus. The other is a KAM torus that cannot be represented as a graph over either the horizontal domain, or even some subset of the horizontal domain. Such KAM tori exist with a region as “localized circles” and trap regions of fluid. They give rise to what are commonly referred to as “islands”.

Caveat: *In this section we will illustrate many of the ideas with sketches of the stable and unstable manifolds of the hyperbolic points associated with the meandering jet. Generally, we expect the manifolds to have infinite length and to form a very complicated spatial structure. Of course, we can only draw finite lengths of the manifolds but one must take care in drawing conclusions from such partial information. In general, we will only draw enough of the length of the manifolds in a figure to illustrate the particular idea under discussion. Moreover, it is tempting to think of the manifolds as “growing” or being created through iteration of finite length segments. This impression stems from the way manifolds are simulated by computer. This is just a way of visualizing the manifolds. They exist in all their full glory and infinite length despite the fact that we cannot draw such a picture or numerically simulate it. Also, since we are considering an area preserving Poincaré map (i.e., incompressible fluid mechanics) as lobes evolve in time that should maintain their area. This requirement may appear to be violated in our sketches, but this is only for the sake of artistic clarity.*

3.1 The Turnstile Mechanism for Fluid Exchange

The segments of stable and unstable manifolds between the boundary intersection point and its inverse under f forms two *lobes*, which are referred to as *turnstile lobes*¹. These lobes are special in the sense that they completely determine the problem of transport between the different regions defined above. We show only the turnstile lobes in Fig. 4, and their images under the Poincaré map in Fig. 5.

Hence, the flux of particles between adjacent regions after one iteration of the map is just the area of the turnstile lobes entering the region. Moreover, the following deeper statement is also true.

The only points that can leave R_i and enter R_j under one iterate of f are those in the turnstile lobe $L_{i,j}$.

This is a significant statement because it says that trajectories can make transitions between different regions only at certain points in space, and it tells us how to locate those points in space. In addition, it enables us to understand a number of transport issues associated with the meandering jet that cannot be addressed with any other methods other than “brute force”, i.e., integrating as many trajectories as are affordable. Mass conservation places a constraint on the turnstile lobes controlling access to adjacent regions. Since $\mu(L_{i,j})$ and $\mu(L_{j,i})$ are the amounts of fluid exchanged under one iteration between regions R_i and R_j , since mass is conserved one must also have:

$$\mu(L_{i,j}) = \mu(L_{j,i}) . \tag{10}$$

We now consider some transport issues in detail.

3.2 Transport Across the Jet

Can trajectories starting in the northern region of recirculating trajectories (R_2) cross the jet (R_3) and enter the southern region of recirculating trajectories (R_4)?

¹It is possible for there to be more than two lobes between a given intersection point and its preimage, as can be seen in figure 12, where $L_{2,3}$ and $L_{3,2}$ are each made of two distinct parts. These technical details are discussed in Wiggins [1992].

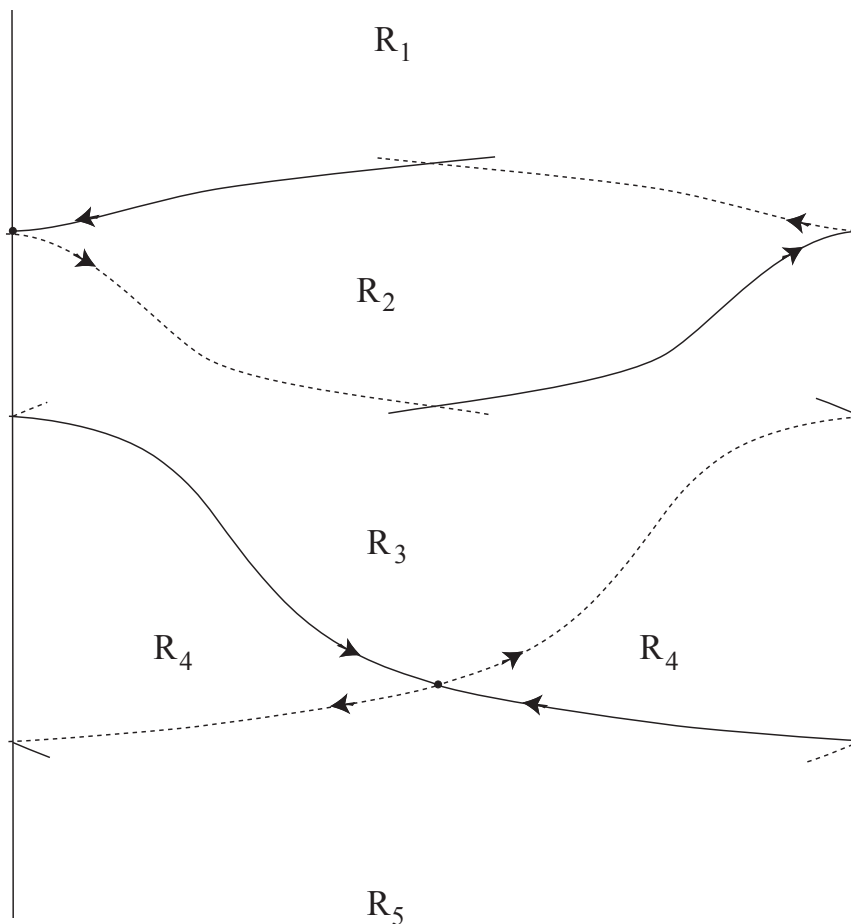


Figure 3: Different regions associated with the jet. The unstable manifolds are shown as dashed lines and the stable manifolds are shown as solid lines. The entire structure is periodic in the horizontal coordinate.

This question is generally posed in relation to the question of the existence of a “barrier to transport” in the jet. Typically, this is a KAM torus, whose existence is difficult to verify rigorously numerically. The question, as we have posed it, can be answered entirely in terms of the dynamics of the turnstiles controlling access to R_2 and R_3 and, if the answer is affirmative, it rigorously rules out the existence of a flow barrier.

Fluid can pass from R_2 into R_3 only through the turnstile lobe $L_{2,3}$. Fluid can pass from R_3 into R_4 only through the turnstile lobe $L_{3,4}$. Hence, a necessary and sufficient condition for fluid to pass from R_2 into R_4 is for $f^m(L_{2,3})$ to intersect $f^{-n}(L_{3,4})$, for some $m, n \geq 0$. This is illustrated in Fig. 6 for $m = 2, n = 1$.

Computationally this is rather easy to verify because it involves only tracking a finite length segment of stable and unstable manifolds that form the boundaries of the relevant turnstile lobes. If there is no barrier to trajectories crossing the jet we can ask another related question.

What route (in space) do trajectories take in crossing the jet in a given time?

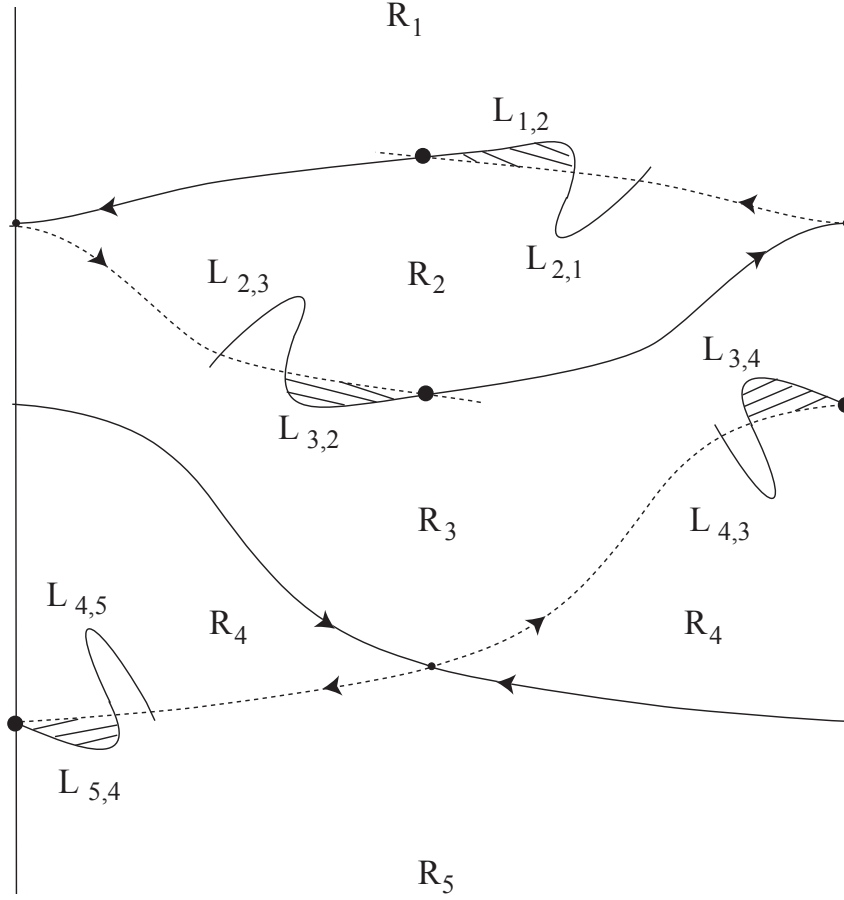


Figure 4: The turnstiles of the different regions associated with the jet.

This question can be answered by elaborating on the discussion above. If $f^m(L_{2,3})$ intersects $f^{-n}(L_{3,4})$, for some $m, n \geq 0$, it follows that $f^{n+m}(L_{2,3})$ intersects $L_{3,4}$. In other words, some iterate of the turnstile lobe that mediates transport between R_2 and R_3 intersects the turnstile lobe that mediates transport between R_3 and R_4 . From this we can determine the spatial structure of the “route” that points must take as they cross the jet from north to south in a certain time. If we define $\mathcal{C} \equiv f^{n+m}(L_{2,3}) \cap L_{3,4}$, then $f^{-(n+m)}(\mathcal{C}) \subset L_{2,3}$. Therefore $f^{-(n+m)}(\mathcal{C})$ enters the jet under one iterate of f , and under further iteration it crosses the jet. After $n + m$ iterates it intersects $L_{3,4}$, and in the next iterate it leaves the jet, exiting into R_4 . Hence the sets:

$$f^{-(n+m)}(\mathcal{C}), f^{-(n+m-1)}(\mathcal{C}), \dots, f^{-1}(\mathcal{C}), \mathcal{C}, \quad (11)$$

denote the spatial “route” that points must pass through as they exit R_2 through the turnstile lobe $L_{2,3}$ and

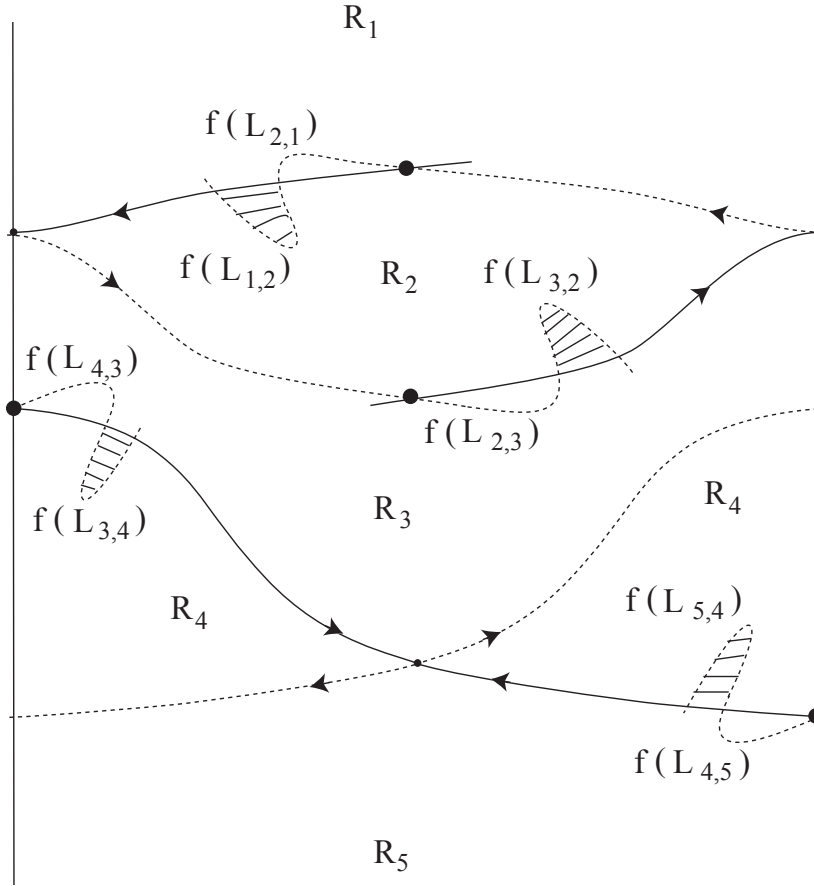


Figure 5: The image of the turnstile lobes under the action of the Poincaré map. The cross-hatched lobes in Fig. 4 correspond to the cross-hatched lobes in this figure. This indicates how the turnstile lobes transport fluid between adjacent regions.

make their way across the jet before exiting the jet through the lobe $f(L_{3,4})$ after $n + m + 1$ iterates. This is illustrated in Fig. 7, which is the same as Fig. 6, with some additional lobes drawn (recall our caveat at the beginning of this section).

3.2.1 Statistical Quantities from Lobe Dynamics Associated with Crossing the Jet

We will now derive some statistical quantities from lobe dynamics associated with crossing the jet. These are simple modifications of results obtained by Meiss [1997] that are adapted for this geometrical set-up. For definiteness, we will consider crossing from north to south. The necessary modifications of our results to consider crossing in the opposite direction should be clear.

We need to define a few notions to deal with averages. Let μ denote Lebesgue measure on the plane. Practically speaking, for us it will just be the function that assigns the area to a given set. Let $f(x)$ denote a (scalar valued) function on the plane, and let S denote a subset of the plane. Then the average of f over

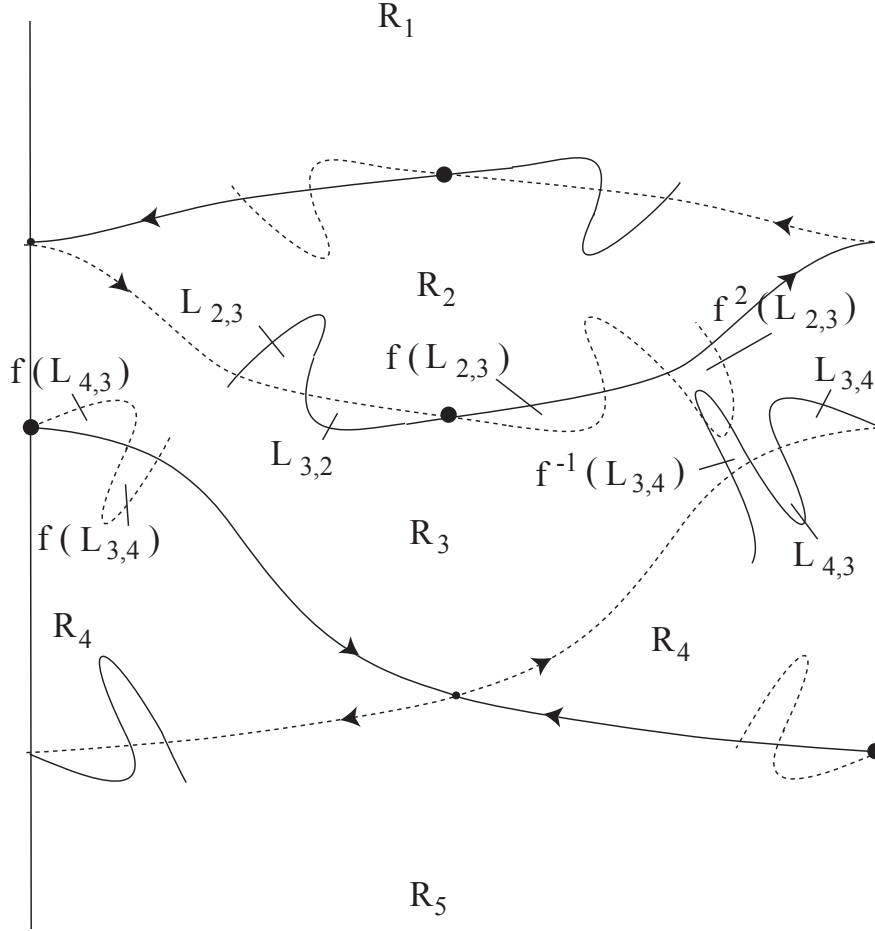


Figure 6: The mechanism for transport across the jet: $f^2(L_{2,3})$ intersects $f^{-1}(L_{3,4})$.

S is defined as:

$$\langle f \rangle_S \equiv \frac{1}{\mu(S)} \int_S f(x) d\mu. \quad (12)$$

First, recall from the discussion above that:

$$f^{-j}(L_{3,4}) \cap L_{2,3}, \quad j \geq 0, \quad (13)$$

are the points that enter the jet from the north, cross it in j iterates, and exit to the south (R_4) on the $j+1$ iterate. Then

$$L_{2,3}^{n,s} \equiv \bigcup_{j=1}^{\infty} (f^{-j}(L_{3,4}) \cap L_{2,3}), \quad (14)$$

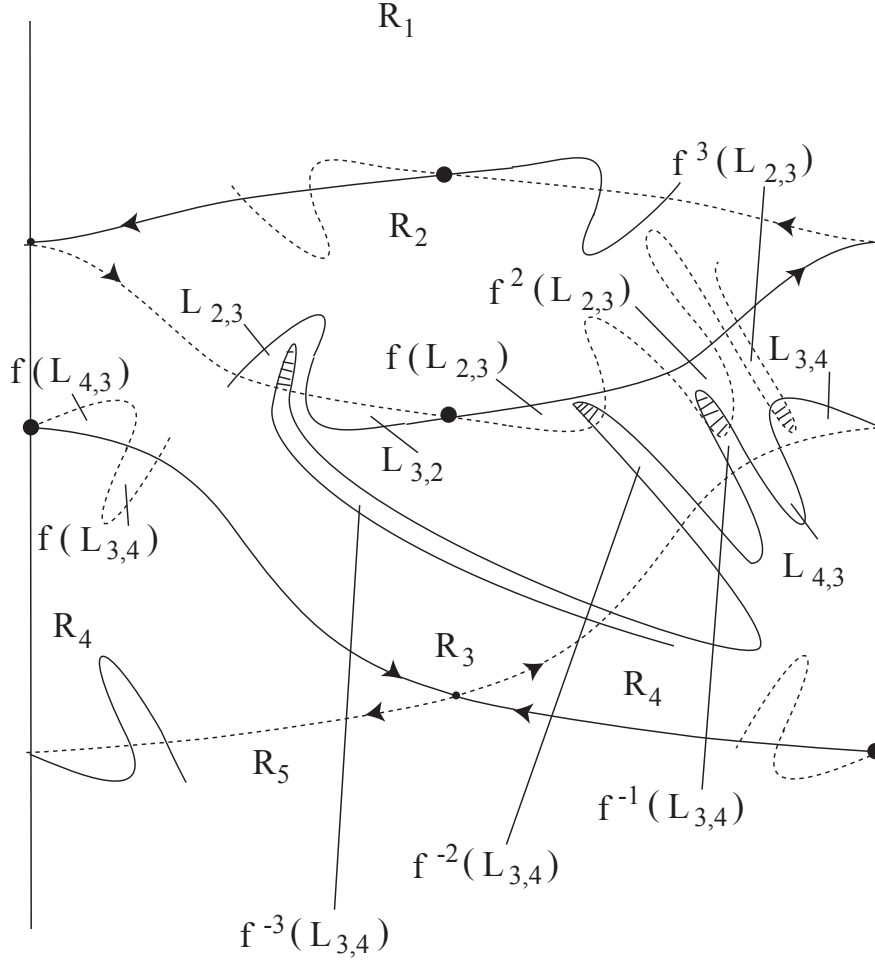


Figure 7: The hatched regions denote points that enter the jet from R_2 , cross the jet, and enter into R_4 . The hatched regions are the sets defined in (11).

are the points in $L_{2,3}$ that enter the jet from the north, cross the jet, and exit to R_4 .

In order to simplify notation we drop the subscripts 2,3 and just denote $\mu(L^{n,s})$ the measure of the set of points in $L_{2,3}$ that enter the jet from the north, cross the jet, and exit to R_4 , i.e.,

$$\mu(L^{n,s}) = \sum_{j=1}^{\infty} \mu(f^{-j}(L_{3,4}) \cap L_{2,3}). \quad (15)$$

We will exploit this notational simplification in analogous quantities that we will derive later.

It follows from equation (14) that the sets:

$$f^i(f^{-j}(L_{3,4}) \cap L_{2,3}), \quad i = 1, \dots, j. \quad (16)$$

are the points *within the jet* that started in R_2 , cross from north to south, and enter R_4 on the $j + 1$ iterate. Hence,

$$X^{n,s} \equiv \bigcup_{j=1}^{\infty} \bigcup_{i=1}^j f^i (f^{-j}(L_{3,4}) \cap L_{2,3}), \quad (17)$$

is the set of points in the jet that has entered from the north, crosses the jet, and exits to the south². In other words, this is the spatial structure within the jet through which particles crossing from north to south must pass.

We have the following result.

Theorem 3.1 *The average time to cross the jet and exit into R_4 for trajectories in $L_{2,3}$ is:*

$$\langle t^{n,s} \rangle = 1 + \frac{\mu(X^{n,s})}{\mu(L^{n,s})}. \quad (18)$$

Proof: The measure of the set of points in $L_{2,3}$ that takes time $j + 1$ iterations to cross the jet from north to south, exiting into R_4 , is $\mu(f^{-j}(L_{3,4}) \cap L_{2,3})$. Therefore, by definition we have:

$$\langle t^{n,s} \rangle = \frac{1}{\mu(L^{n,s})} \sum_{j=1}^{\infty} (j + 1) \mu(f^{-j}(L_{3,4}) \cap L_{2,3}). \quad (19)$$

From (17) we have (using the fact that (13) are disjoint):

$$\mu(X^{n,s}) = \sum_{j=1}^{\infty} \sum_{i=1}^j \mu(f^i (f^{-j}(L_{3,4}) \cap L_{2,3})). \quad (20)$$

Since the Poincaré map is area-preserving we have:

$$\mu(f^i (f^{-j}(L_{3,4}) \cap L_{2,3})) = \mu(f^{-j}(L_{3,4}) \cap L_{2,3}),$$

and this sum becomes:

$$\mu(X^{n,s}) = \sum_{j=1}^{\infty} j \mu(f^{-j}(L_{3,4}) \cap L_{2,3}), \quad (21)$$

which, upon substituting into (19), and using (15), gives the result. Note that since $\mu(X^{n,s}) \leq \mu(R_3)$ the sum converges. \square

This is an interesting result in that it expresses the average crossing time entirely in terms of lobe dynamics. The fact that (21) converges leads to the following corollary.

Corollary 3.1 *The measure of the set of points in $L_{2,3}$ that crosses the jet and escapes to the south in $j + 1$ iterations goes to zero at least as fast as j^{-2} as $j \rightarrow \infty$.*

A similar theorem and corollary can be given for particles crossing the jet from the south to the north.

3.3 Trajectories that Enter the Jet, but Do Not Cross the Jet

For definiteness we consider trajectories that enter the jet from the north. A similar argument applies to trajectories entering the jet from the south.

Trajectories can only enter the jet from the north through the turnstile lobe $L_{2,3}$. As this lobe evolves in time it may intersect one of the pre-images of $L_{3,2}$. These points will then re-enter R_2 .

²The superscripts on $X^{n,s}$ (“X” is meant to denote “crossing”) explicitly denote the manner of crossing. The left most superscript (“n”) denotes the fact that the point starts in the north. The right most superscript (“s”) denotes the fact that the point moves to the south.

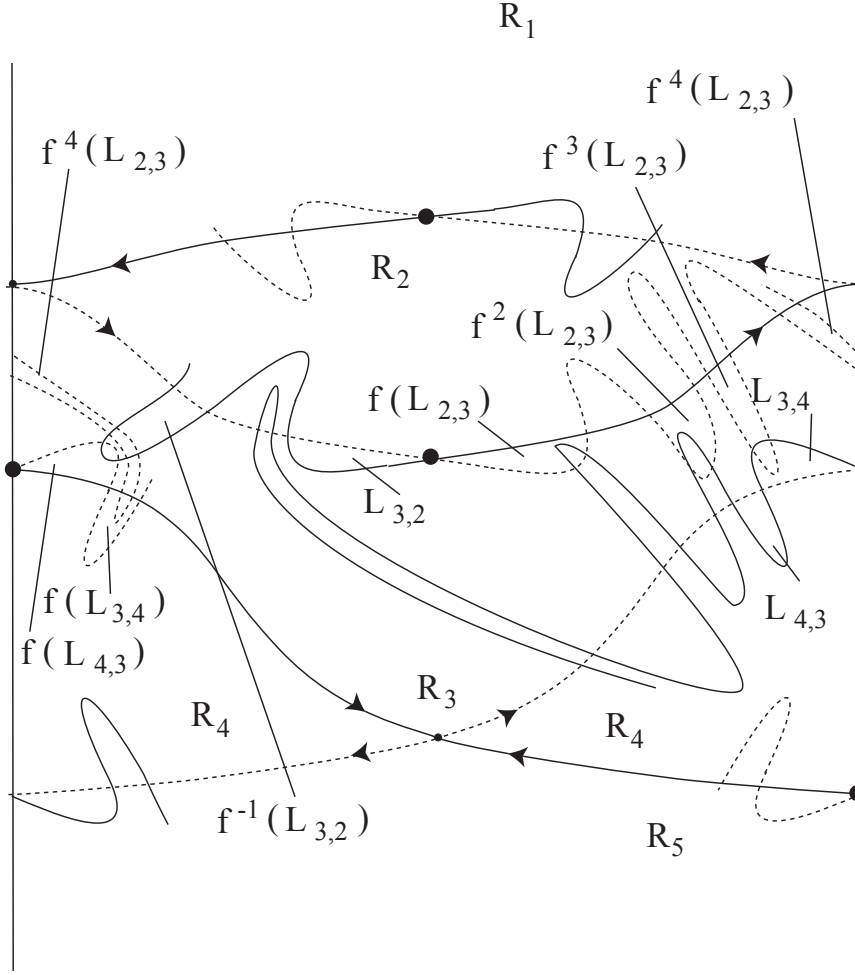


Figure 8: The mechanism for particles to enter the jet from the north, and then exit the jet to the north.

3.3.1 Statistical Quantities Associated with Particles that Enter the Jet, but do Not Cross the Jet

As above, these are simple modifications of results obtained by Meiss [1997] that are adapted for this geometrical set-up.

It follows from the discussion above that:

$$f^{-j}(L_{3,2}) \cap L_{2,3}, \quad j \geq 1, \quad (22)$$

are the points that enter the jet from R_2 , and then exit it by re-entering R_2 in $j + 1$ iterates. Then

$$L_{2,3}^{n,n} \equiv \bigcup_{j=1}^{\infty} (f^{-j}(L_{3,2}) \cap L_{2,3}), \quad (23)$$

is the set of points in $L_{2,3}$ that enter the jet, and then exit at some time later by exiting to the north (back into R_2). Adopting the simpler notation introduced in the last section (i.e., dropping subscripts), the measure of this set of points is given by:

$$\mu(L^{n,n}) = \sum_{j=1}^{\infty} (f^{-j}(L_{3,2}) \cap L_{2,3}). \quad (24)$$

It follows that the sets:

$$f^i (f^{-j}(L_{3,2}) \cap L_{2,3}), \quad i = 1, \dots, j. \quad (25)$$

are the points *in the jet* that have entered from R_2 and exit into R_2 in $j + 1$ iterates. Hence,

$$X^{n,n} \equiv \bigcup_{j=1}^{\infty} \bigcup_{i=1}^j f^i (f^{-j}(L_{3,2}) \cap L_{2,3}), \quad (26)$$

Similarly as before, the following equality holds:

$$\mu(X^{n,n}) = \sum_{j=1}^{\infty} j \mu(f^{-j}(L_{3,2}) \cap L_{2,3}), \quad (27)$$

is the set of points in the jet that has entered from the north and exits to the north. In other words, it is the spatial structure within the jet through which particles must pass if they enter the jet from the north (R_2), and do not cross the jet, but exit the jet later to the north (R_2).

Theorem 3.2 *The average time for trajectories starting in $L_{2,3}$ to enter the jet and later exit the jet to the north is:*

$$\langle t^{n,n} \rangle = 1 + \frac{\mu(X^{n,n})}{\mu(L^{n,n})}. \quad (28)$$

A corollary on convergence holds exactly as above.

Corollary 3.2 *The measure of the set of points in $L_{2,3}$ that enters the jet and escapes to the north in $j + 1$ iterations goes to zero at least as fast as j^{-2} as $j \rightarrow \infty$.*

A similar theorem and corollary can be given for particles entering the jet from the south and escaping back to the south can also be stated and proved. As we mentioned earlier, a study of the asymmetry (or symmetry) between these two transport issues is possible with the techniques introduced here.

3.4 Geometrical Constraints on Lobe Dynamics

We demonstrate here the existence of exact relations between the quantities introduced above. These relations will be used in the following sections.

3.4.1 Exact relations between $\mu(L^{n,s})$, $\mu(L^{n,n})$, $\mu(L^{s,n})$ and $\mu(L^{s,s})$.

As one can see, formulae (15) and (24) are expressed in terms of sums of the area of intersection of $L_{2,3}$ with either $f^{-j}(L_{3,4})$ or $f^{-j}(L_{3,2})$ (for some $j > 1$), depending on whether a point in this intersection will leave the jet by the south or by the north, respectively. Indeed, any point that enters region R_3 from the north, will leave it by either the north or by the south. Hence we obtain the first geometrical constraint:

$$\mu(L^{n,s}) + \mu(L^{n,n}) = \mu(L_{2,3}).$$

Basically, this is just another way of stating that points that enter from the north enter from $L_{2,3}$. By similar reasoning, we obtain three other equations:

$$\begin{aligned}
\mu(L^{s,n}) + \mu(L^{s,s}) &= \mu(L_{4,3}) , \\
\mu(L^{n,n}) + \mu(L^{s,n}) &= \mu(L_{3,2}) , \\
\mu(L^{n,s}) + \mu(L^{s,s}) &= \mu(L_{3,4}) ,
\end{aligned}$$

which state, respectively, that points that enter from the south enter from $L_{4,3}$, points that leave the jet to the north exit through $L_{3,2}$, and points that exit the jet to the south exit through $L_{3,4}$.

Now the areas of the turnstile lobes are fairly easy to compute. Therefore if we view the turnstile lobe areas as “known,” we have obtained four equations for the four unknowns, $\mu(L^{s,n}), \mu(L^{n,s}), \mu(L^{n,n}), \mu(L^{s,s})$.

However, these equations are not all independent. Since $\mu(L_{2,3}) = \mu(L_{3,2})$ and $\mu(L_{4,3}) = \mu(L_{3,4})$ it follows that we have:

$$\mu(L^{n,s}) = \mu(L^{s,n}) , \quad (29)$$

and the four equations above reduce to the following two independent equations:

$$\mu(L^{n,s}) + \mu(L^{n,n}) = \mu(L_{2,3}) , \quad (30)$$

$$\mu(L^{s,n}) + \mu(L^{s,s}) = \mu(L_{4,3}) . \quad (31)$$

3.4.2 Exact relations between $\mu(X^{n,s}), \mu(X^{n,n}), \mu(X^{s,n})$ and $\mu(X^{s,s})$.

Another type of geometrical constraint is somewhat less straightforward, and we will explain it here. Consider a point in R_3 : we ask if it remains in R_3 forever under iteration, or does it leave R_3 after a finite number of iterations, either by the south or by the north? In part II, we will show how one can construct a generalized horseshoe map inside R_3 . Therefore, a point that remains in R_3 forever either belongs to a region enclosed by a KAM torus, or it belongs to the invariant set associated with a horseshoe map (“chaotic saddle”) in R_3 (which has Lebesgue measure is zero). We define R_3^* as the set of points inside R_3 that are *not* contained inside a KAM torus (this means, the points inside R_3 that either belong to the chaotic saddle or those that leave R_3 after a finite number of iterations). Now by our earlier discussions any point that will leave R_3 has to belong either to $X^{n,n}$, or to $X^{n,s}$, or to $X^{s,s}$, or to $X^{s,n}$. Of course, all these sets have zero intersection (a point that crosses from north to south can not also cross from north to north, for instance). Hence, since the chaotic saddle has zero Lebesgue measure, we must have the following geometrical constraint:

$$\mu(X^{n,s}) + \mu(X^{n,n}) + \mu(X^{s,n}) + \mu(X^{s,s}) = \mu(R_3^*) . \quad (32)$$

Now, let us further consider the fate of points in R_3 : because of mass conservation, the mass of fluid that enters from the north must be equal to the mass that exits to the north, i.e.,

$$\mu(X^{n,s}) + \mu(X^{n,n}) = \mu(X^{n,n}) + \mu(X^{s,n}) ,$$

and we obtain:

$$\mu(X^{n,s}) = \mu(X^{s,n}) . \quad (33)$$

3.4.3 North–South versus South–North Crossing Statistics

It follows from (29) and (33) that we have the following result:

$$\langle t^{n,s} \rangle = \langle t^{s,n} \rangle . \quad (34)$$

Therefore, the mean statistics for north–south crossing are the same as for south–north crossing. However, we emphasize that having equal means does not mean that north–south and south–north crossing statistics are completely symmetric –although they are indeed in the cases when $\epsilon_2 = 0$, as discussed previously in section 2–.

3.5 Mean Residence Time and Escape from the Jet

3.5.1 Mean Residence Time in the Jet

Up to now, we have only dealt with particles that follow a particular route inside R_3 (from north to south, north to north, etc). We can also deduce the mean residence time inside region R_3 , $\langle t_{R_3} \rangle$, as follows³:

Theorem 3.3

$$\langle t_{R_3} \rangle = \frac{\mu(X^{n,s}) + \mu(X^{n,n}) + \mu(X^{s,n}) + \mu(X^{s,s})}{\mu(L_{2,3}) + \mu(L_{4,3})} \quad (35)$$

$$= \frac{\mu(R_3^*)}{\mu(L_{2,3}) + \mu(L_{4,3})}. \quad (36)$$

Proof: The proof is similar to that of Theorem 3.1: the measure of the set of points in $L^{n,s}$ that takes time $j+1$ iterations to cross the jet from north to south, exiting into R_4 , is $\mu(f^{-j}(L_{3,4}) \cap L_{2,3})$. Therefore, the measure of the set of points in $L^{n,s}$ that come from the north and escape to the south and remain inside R_3 for j iterations is $\mu(f^{-j}(L_{3,4}) \cap L_{2,3})$. In order to determine the mean time inside R_3 for all points we must also take into account points that cross the jet from south to north, or points that enter from the north and leave by the north, or points that enter from the south and leave by the south. The measure of the set of points of $L_{2,3}$ or $L_{4,3}$ that remain inside the jet during j periods is $\mu(f^{-j}(L_{3,4}) \cap L_{2,3}) + \mu(f^{-j}(L_{3,4}) \cap L_{4,3}) + \mu(f^{-j}(L_{3,2}) \cap L_{2,3}) + \mu(f^{-j}(L_{3,2}) \cap L_{4,3})$. Therefore, by definition we have:

$$\langle t_{R_3} \rangle = \frac{\sum_{j=1}^{\infty} j [\mu(f^{-j}(L_{3,4}) \cap L_{2,3}) + \mu(f^{-j}(L_{3,4}) \cap L_{4,3}) + \mu(f^{-j}(L_{3,2}) \cap L_{2,3}) + \mu(f^{-j}(L_{3,2}) \cap L_{4,3})]}{\mu(L^{n,s}) + \mu(L^{n,n}) + \mu(L^{s,n}) + \mu(L^{s,s})}. \quad (37)$$

Using the definitions of $X^{n,s}$, $X^{n,n}$, $X^{s,n}$, $X^{s,s}$, one easily obtains eq. (36). \square

In general, the same reasoning as above will apply to any region of the flow. Hence, the mean residence time in region R_i is simply given by

$$\langle t_{R_i} \rangle = \frac{\mu(R_i^*)}{\sum_{j \neq i} \mu(L_{j,i})}, \quad (38)$$

where $\mu(R_i^*)$ is the area occupied by trajectories that leave region R_i after finite time; therefore, if region R_i is bounded (or periodic in a direction in which it is not bounded, like region R_3), it is possible to have an upper bound for the associated residence time,

$$\langle t_{R_i} \rangle \leq \frac{\mu(R_i)}{\sum_{j \neq i} \mu(L_{j,i})}. \quad (39)$$

It is significant to note that the mean residence time in a region does not depend on the decay rate (algebraic or exponential) inside this region, but is just given by the area of the chaotic zones and lobes.

3.5.2 Escape from the Jet

Suppose that the fluid inside the jet at $t=0$ (region R_3) has been marked: how rapidly does this marked fluid escape from this region? Answering this question poses some difficulties: suppose that inside R_3 there exists a regular island ($R_3^* \neq R_3$); then if we fill region R_3 with marked fluid some of it will never escape from R_3 . Therefore, it becomes difficult to decide numerically when to stop integrating trajectories for a large number of points distributed uniformly throughout the region. Using Lobe Dynamics, we can answer this question numerically, just by following the fluid initially inside $L_{2,3}$ and $L_{4,3}$ (and this is much less effort than is required for following points filling the entire region R_3).

³Note that the mean time required to leave region R_3 , once it has been entered, is $1 + \langle t_{R_3} \rangle$

At period i , the fluid that escapes from R_3 was inside $L_{3,4}$ or $L_{3,2}$ at period $i-1$. From this quantity we must take away the unmarked fluid that may have entered the jet from regions R_2 or R_4 earlier. Therefore, at period i the quantity of marked fluid that leaves the jet is:

$$\begin{aligned} \mu(L_{3,4}) & - \sum_{j=1}^{i-1} \mu[f^j(L_{2,3}) \cap L_{3,4}] & - \sum_{j=1}^{i-1} \mu[f^j(L_{4,3}) \cap L_{3,4}] \\ + \mu(L_{3,2}) & - \sum_{j=1}^{i-1} \mu[f^j(L_{2,3}) \cap L_{3,2}] & - \sum_{j=1}^{i-1} \mu[f^j(L_{4,3}) \cap L_{3,2}]. \end{aligned} \quad (40)$$

Because of area conservation, $\mu[f^j(L_{2,3}) \cap L_{3,4}] = \mu[f^{-j}(L_{3,4}) \cap L_{2,3}]$ and we recognize here a truncated series of the infinite series defining $\mu(L^{n,s})$, $\mu(L^{n,n})$, $\mu(L^{s,n})$ and $\mu(L^{s,s})$. Therefore the quantity of fluid that leaves at iteration i is

$$\mu(L_{3,4}) + \mu(L_{3,2}) - \mu_{-}L^{n,s}(i-1) - \mu_{-}L^{n,n}(i-1) - \mu_{-}L^{s,n}(i-1) - \mu_{-}L^{s,s}(i-1), \quad (41)$$

where the truncated series of $\mu(L^{n,s})$ at iteration i is defined as follows:

$$\mu_{-}L^{n,s}(i) = \sum_{j=1}^i \mu(f^{-j}(L_{3,4}) \cap L_{2,3}), \quad (42)$$

and similar definitions hold for $\mu_{-}L^{n,n}(i)$, $\mu_{-}L^{s,n}(i)$ and $\mu_{-}L^{s,s}(i)$. Using equation (41), the amount of marked fluid that has escaped after ℓ iterates can be easily computed; it is exactly:

$$\sum_{i=1}^{\ell} [\mu(L_{3,4}) + \mu(L_{3,2}) - \mu_{-}L^{n,s}(i-1) - \mu_{-}L^{n,n}(i-1) - \mu_{-}L^{s,n}(i-1) - \mu_{-}L^{s,s}(i-1)]. \quad (43)$$

3.5.3 The limit $\ell \rightarrow \infty$

In order to be consistent, we must check that:

Theorem 3.4 *As time goes to infinity the total amount of marked fluid that escapes from R_3 is $\mu(R_3^*)$, i.e. when taking the limit $\ell \rightarrow \infty$ in equation (43), one recovers $\mu(R_3^*)$:*

$$\sum_{i=1}^{\infty} [\mu(L_{3,4}) + \mu(L_{3,2}) - \mu_{-}L^{n,s}(i-1) - \mu_{-}L^{n,n}(i-1) - \mu_{-}L^{s,n}(i-1) - \mu_{-}L^{s,s}(i-1)] = \mu(R_3^*). \quad (44)$$

Proof:

We begin with a lemma:

Lemma 3.1

$$\sum_{i=1}^{\infty} [\mu(L^{n,s}) - \mu_{-}L^{n,s}(i-1)] = \mu(X^{n,s}). \quad (45)$$

Similar equalities exist with $\mu(X^{n,n})$, $\mu(X^{s,n})$ and $\mu(X^{s,s})$.

Proof: Let us introduce the truncated series at step ℓ ,

$$E^{n,s}(\ell) = \sum_{i=1}^{\ell} [\mu(L^{n,s}) - \mu_{-}L^{n,s}(i-1)] \quad (46)$$

$$= \sum_{i=1}^{\ell} \left[\sum_{j=i}^{\infty} \mu(f^{-j}(L_{3,4}) \cap L_{2,3}) \right]. \quad (47)$$

We let $a_j = \mu(f^{-j}(L_{3,4}) \cap L_{2,3})$; We prove by induction that

$$E^{n,s}(\ell) = \sum_{j=1}^{\ell} j a_j + \ell \sum_{j=\ell+1}^{\infty} a_j . \quad (48)$$

For $\ell = 1$, we recover that $E^{n,s}(1) = \sum_{j=1}^{\infty} a_j = \mu(L^{n,s})$ and equation (48) holds. Suppose now that the result is true for a given ℓ ; then

$$E^{n,s}(\ell+1) = E^{n,s}(\ell) + (\mu(L^{n,s}) - \mu_{-}L^{n,s}(\ell)) \quad (49)$$

$$= E^{n,s}(\ell) + \sum_{j=\ell+1}^{\infty} a_j \quad (50)$$

$$= \sum_{j=1}^{\ell} j a_j + \ell \sum_{j=\ell+1}^{\infty} a_j + \sum_{j=\ell+1}^{\infty} a_j \quad (51)$$

$$= \sum_{j=1}^{\ell} j a_j + (\ell+1) a_{\ell+1} + (\ell+1) \sum_{j=\ell+2}^{\infty} a_j \quad (52)$$

$$= \sum_{j=1}^{\ell+1} j a_j + (\ell+1) \sum_{j=\ell+2}^{\infty} a_j \quad (53)$$

Therefore the result is true for $\ell+1$ and therefore by induction equation (48) holds for any ℓ .

We must now prove that $\lim_{\ell \rightarrow \infty} E^{n,s}(\ell) = \mu(X^{n,s})$: from equation (21), $\mu(X^{n,s}) = \sum_{i=1}^{\infty} j a_j$ and the first term in the right hand side of equation (48) converges to $\mu(X^{n,s})$. We now prove that the other term of the right hand side of equation (48) goes to zero as follows: since $a_j \geq 0$ for all j 's, we can write

$$\ell \sum_{j=\ell+1}^{\infty} a_j < \sum_{j=\ell+1}^{\infty} j a_j \quad (54)$$

$$< \mu(X^{n,s}) - \mu_{-}X^{n,s}(\ell), \quad (55)$$

where

$$\mu_{-}X^{n,s}(\ell) = \sum_{j=1}^{\ell} j \mu(f^{-j}(L_{3,4}) \cap L_{2,3}) \quad (56)$$

is the truncated series for $\mu(X^{n,s})$. Since the series $\mu(X^{n,s})$ converges, the right hand side of equation (54) goes to zero as ℓ goes to infinity. Hence, we have proven equality (45). \square

It is now very easy to prove theorem 3.4: we use lemma 45, and the three similar equalities for $\mu(X^{n,n})$, $\mu(X^{s,n})$ and $\mu(X^{s,s})$. When we add these four equations together, we obtain:

$$\begin{aligned} \sum_{i=1}^{\infty} [\mu(L^{n,s}) - \mu_{-}L^{n,s}(i-1) + \mu(L^{n,n}) - \mu_{-}L^{n,n}(i-1) + \mu(L^{s,n}) - \mu_{-}L^{s,n}(i-1) + \mu(L^{s,s}) - \mu_{-}L^{s,s}(i-1)] \\ = \mu(X^{n,s}) + \mu(X^{n,n}) + \mu(X^{s,n}) + \mu(X^{n,n}). \end{aligned} \quad (57)$$

We finally introduce the three geometrical constraints (30), (31), and (32) into equation (57), and the result follows. \square

4 Numerical Results

In this section we present some numerical results for this geometry for different sets of parameters. First of all a finite piece of the stable and unstable manifolds of the Poincaré sections were calculated, together with the Poincaré section of a given point initially in $L_{2,3}$. We then show “exact” results obtained through Monte Carlo simulation, by filling uniformly a given lobe with many initial conditions.

4.1 Set of parameters chosen

We chose a set of fairly large frequency of the perturbation, in which case there is no noticeable exchange between regions R_1 and R_2 , nor between regions R_5 and R_4 (also noted in Samelson [1992]), but there is exchange across the jet from region R_2 to R_4 .

We present here four sets of parameters; in the first and the second ones, denoted thereafter by A and B, we considered only the time periodic meander amplitude perturbation given in (4) (i.e., $\epsilon_2 = 0$). For this type of variability we have a symmetry between north-north transport and south-south transport, and in particular, the areas of the turnstile lobes $\mu(L_{2,3})$ and $\mu(L_{4,3})$ are equal. In the first one chaos seems global in the jet ($\mu(R_3^*) \simeq \mu(R_3)$), while the second example shows the existence of a regular island in the chaotic sea.

In cases C and D, the flow is not symmetric ($\epsilon_2 \neq 0$); in case C some very little island exist inside region R_3 , while in example D the assymetry is very strong but chaos is global inside the jet.

4.1.1 Case A: Full North-South Symmetry ($\epsilon_2 = 0$), with $R_3^* \equiv R_3$

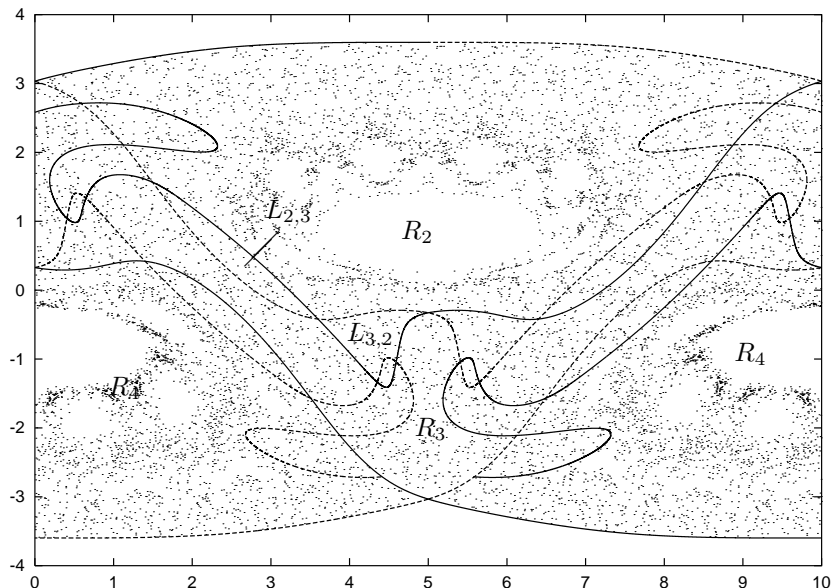


Figure 9: Poincaré section of the meandering jet, for parameters $B = 1.2$, $c = .2$, $\omega = 0.85$ and $\epsilon_1 = 0.9$, $\epsilon_2 = 0$; the initial condition is one point in $L_{2,3}$, and we looked at 10^4 iterates. Although some regular regions appear inside regions R_2 and R_4 , region R_3 appears numerically to be completely chaotic, i.e., $R_3^* \approx R_3$.

Because of the symmetry, one has $\mu(X^{n,n}) = \mu(X^{s,s})$. Moreover, as one can see in figure 9, there appear to be no regular region inside R_3 ; we also checked this numerically, since we found $\mu(X^{n,s}) + \mu(X^{s,n}) = 7.79$, and $\mu(R_3)/2 = 7.8$. Therefore, one can state in this example that $R_3^* \approx R_3$. For this set of parameter we obtained numerically:

$$\begin{aligned} \langle t^{n,s} \rangle &= 11.6 \\ \langle t^{n,n} \rangle &= 12.6 , \end{aligned}$$

while the mean crossing time found using a finite piece of manifolds is

$$\langle t_{R_3} \rangle = \frac{\mu(R_3)}{2 \mu(L_{2,3})} \quad (58)$$

$$= 11.1, \quad (59)$$

and the mean time spent in the jet (R_3) is $1 + \langle t_{R_3} \rangle$, which is indeed in between $\langle t^{n,s} \rangle$ and $\langle t^{n,n} \rangle$; it can be noted that those three values have the same order of magnitude.

4.1.2 Case B: North-South Symmetry ($\epsilon_2 = 0$), but $\mu(R_3^*) < \mu(R_3)$

In this case there is still a north-south symmetry, but chaos is not global inside R_3 ($\mu(R_3^*) < \mu(R_3)$).

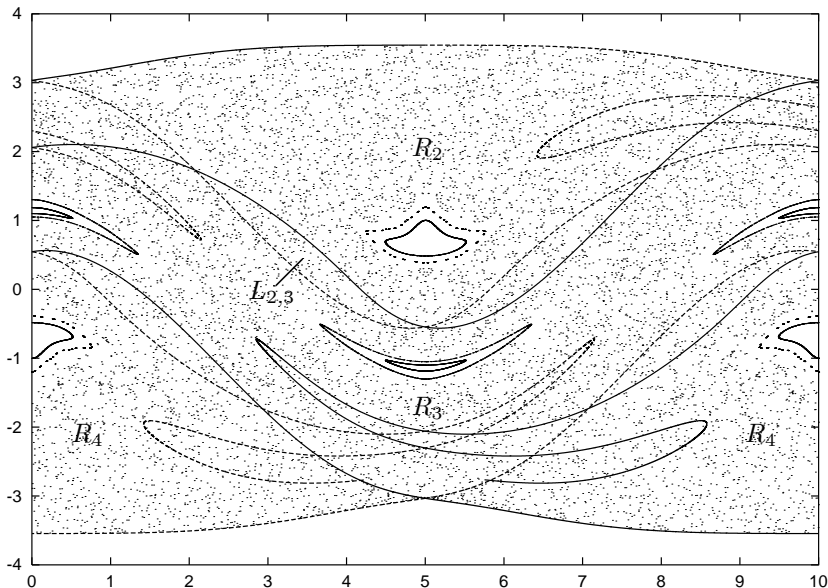


Figure 10: Poincaré section of the meandering jet, for parameters $B = 1.2$, $c = 0.1$, $\omega = 0.4$, $\epsilon_1 = 0.15$, $\epsilon_2 = 0$. we have $\mu(L_{2,3}) = 0.9885$, and $\mu(R_3) = 24.4$ Here region R_3 is clearly not completely chaotic (some islands appear inside the jet), so that $\mu(R_3^*)$, calculated numerically, was found equal to 22.9. .

For this set of parameter we obtained numerically:

$$\langle t^{n,s} \rangle = 16.5$$

$$\langle t^{n,n} \rangle = 10.5,$$

and the mean time spent in the jet is $1 + \mu(R_3^*)/[2\mu(L_{2,3})] = 12.6$. Here there is a 60% difference between north-north and north-south mean crossing times.

4.1.3 Case C: A Non-Symmetric Example with $\mu(R_3^*) \approx \mu(R_3)$

When $\epsilon_2 \neq 0$, the flow still has the symmetry (8) (that symmetry allows us to infer the behavior of the stable manifolds knowing only the unstable manifolds), but does no longer have the symmetry (9). The calculated Poincaré section corresponding to the case $c = 0.1$, $\omega = 0.5$, $\epsilon_1 = 0.45$ and $\epsilon_2 = 0.2$ is shown on figure 11. With the parameters chosen, we obtain $\mu(L_{2,3}) = \mu(L_{3,2}) = 1.68$ and $\mu(L_{3,4}) = \mu(L_{4,3}) = 1.205$, so that $\beta = \mu(L_{3,4})/[\mu(L_{3,4}) + \mu(L_{3,2})] = 0.418$.

In this case chaos is nearly global in region R_3 although little regular regions are visible. We found numerically using the Monte Carlo method that $\mu(R_3^*) = 25.5$, while $\mu(R_3) = 26.1$. The mean residence time

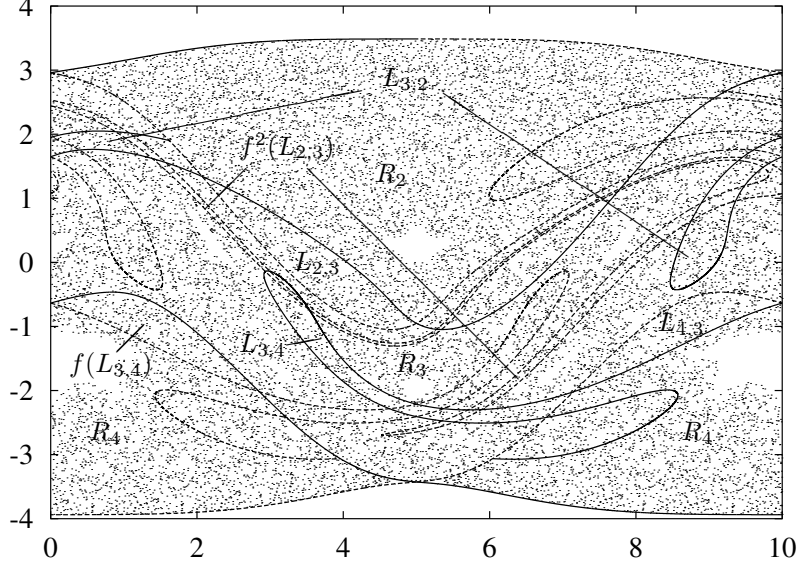


Figure 11: Computed manifolds for the meandering jet for parameters $c = 0.1$, $\omega = 0.5$, $\epsilon_1 = 0.45$ and $\epsilon_2 = 0.2$: $f^2(L_{2,3})$ intersects $L_{3,4}$ twice. Therefore fluid exchange is possible in between regions R_2 and R_4 . Here $\mu(L_{2,3}) \neq \mu(L_{4,3})$: the north-south symmetry is broken. Note also that some very small regular regions exist inside region R_3 . The Poincaré section was computed for an initial condition inside $L_{2,3}$, for $2 \cdot 10^4$ iterations, so as to make those zones visible.

in R_3 is given by eq. (38) and we obtain $\langle t_{R_3} \rangle = \mu(R_3^*) / [\mu(L_{2,3}) + \mu(L_{4,3})] = 8.84$ (and the mean crossing time is $1 + \langle t_{R_3} \rangle = 9.84$). We found numerically that

$$\begin{aligned} \langle t^{n,s} \rangle &= 10 \\ \langle t^{n,n} \rangle &= 9.3 \\ \langle t^{s,s} \rangle &= 10.7 ; \end{aligned}$$

in this case, like in case A, those three values have the same order of magnitude.

4.1.4 Case D: An even less symmetric example

We now consider a completely asymmetric case, for which the associated Poincaré section is shown in figure 12. We found numerically that

$$\begin{aligned} \langle t^{n,s} \rangle &= 14.3 \\ \langle t^{n,n} \rangle &= 11.9 \\ \langle t^{s,s} \rangle &= 12.9 \\ \text{and } 1 + \langle t_{R_3} \rangle &= 13.5 . \end{aligned}$$

In this example again, all those results fall in the same range. that is, most of time, $1 + \langle t_{R_3} \rangle$ gives a good order of magnitude for the different crossing times.

4.2 Escape from the jet

We present here some results on escape from the jet that can be found only numerically using a Monte-Carlo method (while the mean residence time could be found with only a finite piece of manifolds); as we will show, the escape rate is not always exponential. moreover, we will derive an interesting property from the statistics of exit times that we will use in the next section.

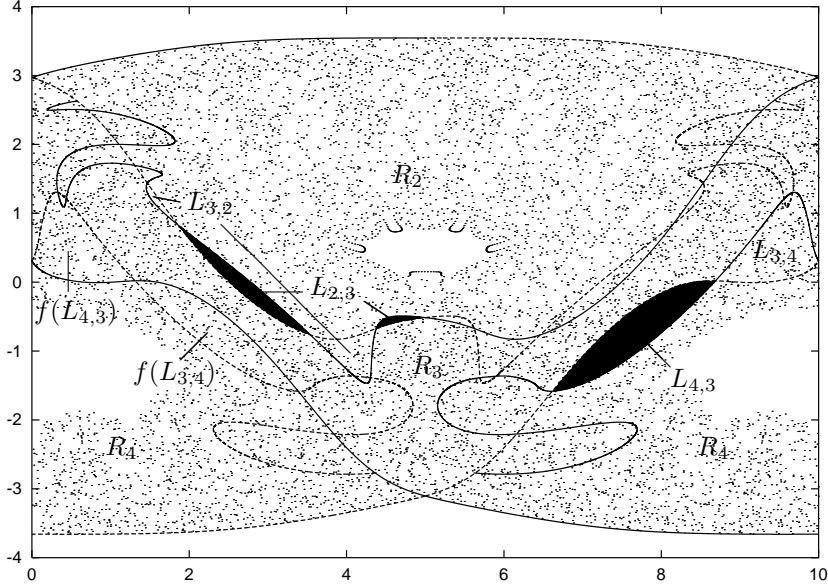


Figure 12: Computed set of manifolds for the double-perturbed meandering jet for parameters $c = 0.2$, $\omega = 0.85$, $\epsilon_1 = 0.9$ and $\epsilon_2 = 0.15$: Here $L_{2,3}$ is made of two distinct parts. Its area is much smaller than that of $L_{4,3}$. Here $\mu(R_3) = 15.6$, $\mu(L_{4,3}) = 0.9077$, $\mu(L_{2,3}) = 0.3399$

4.2.1 Statistics of exit times

Instead of only calculating the mean exit times ($\langle t^{n,s} \rangle$, $\langle t^{n,n} \rangle$, ...), we present in figures 13A–D the full statistics of exit times for fluid initially in the turnstile lobe $L_{2,3}$. For each set of parameters, we show the statistics of the number of points –divided by the total number of points initially in $L_{2,3}$ – that exit by the north (solid boxes) or by the south (dotted boxes), as a function of the number of periods (dimensionless time) . It can be seen that the statistics for fluid leaving by the south or the north are clearly proportional for moderate times; the coefficient of proportionality is equal to $\mu(L_{3,4})/\mu(L_{3,2})$ (i.e. equal to 1 in cases A and B). D. Del-Castillo-Negrete [1998] studied transport of passive scalar in a chain of vortices in a shear layer, using a model motivated by the quasigeostrophic equation; in this geometry he found that the PDFs of the duration of flight (motion following the shear flow) events, and vortex trapping events, both exhibited algebraic decay. It is interesting to note that in the meandering jet geometry, in all the cases with possible mass exchange between north and south, we never found this type of behaviour in the central region R_3 : only in the cases where a regular island existed inside the jet were the statistics of exit times not exponential for large times (although not algebraic either). This property will be seen also later in the decay rate inside the jet.

4.2.2 The well-mixed hypothesis

We explain now why the statistics of exit times by the south or by the north are proportional: as described earlier, at period j , the quantity of fluid initially in $L_{2,3}$ that escapes into region R_4 is $\mu[f^{j-1}(L_{2,3}) \cap L_{3,4}]$, while the quantity of fluid that escapes into region R_2 is $\mu[f^{j-1}(L_{2,3}) \cap L_{3,2}]$. Involving the areas of the intersection of the same lobe $f^{j-1}(L_{2,3})$ with the turnstile lobe $L_{3,4}$ for fluid escaping by the south, and the turnstile lobe $L_{3,2}$ for fluid escaping by the north. For moderate⁴ up to large j , $f^j(L_{2,3})$ is a thin filament that intersects both $L_{3,2}$ and $L_{3,4}$ many times. The well-mixed hypothesis supposes that $f^j(L_{2,3})$ is well mixed in the R_3 regions so that the area of the intersection of $f^{j-1}(L_{2,3})$ with either $L_{3,2}$ and $L_{3,4}$ is controlled by the ratio of lobe areas.

⁴By moderate we mean that j must be larger than the smallest k such that $f^k(L_{2,3}) \cap L_{3,4} \neq \emptyset$, and also larger than the smallest m such that $f^m(L_{2,3}) \cap L_{3,2} \neq \emptyset$.

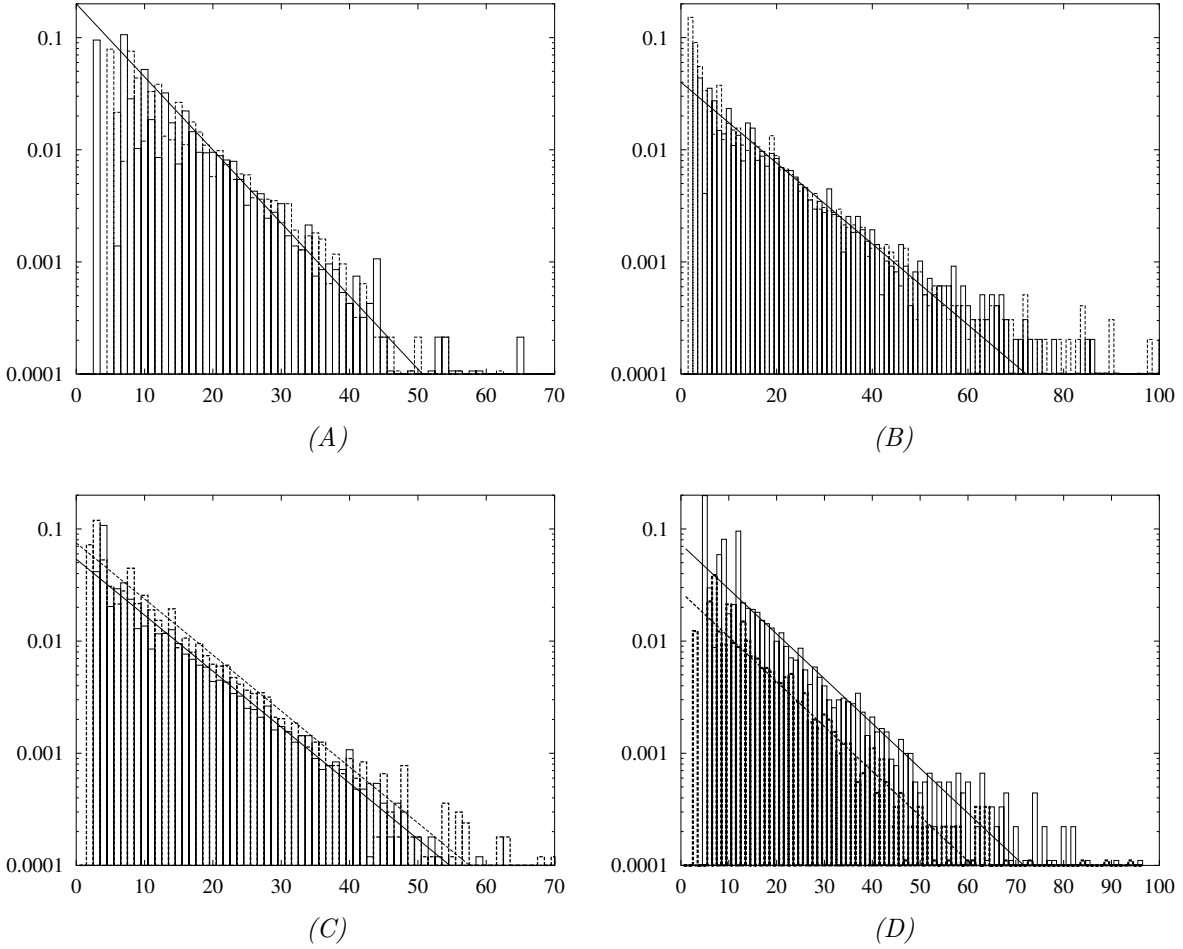


Figure 13: Full statistics of exit times in the four sets of parameters A–D. The calculations were performed using a Monte-Carlo method, by filling uniformly $L_{2,3}$ with a large number of points (around 10^4). The number of points leaving by the north, divided by the total number of points initially in $L_{2,3}$, as a function of the number of periods, are in solid boxes; those with dotted boxes represent the statistics of exit time of points leaving by the south. In the four cases, the decay is exponential for short times. In cases B and C however, some points did exit region R_3 at quite long times, although we did not show it in those figures. In the two symmetric cases A and B, the statistics of south and north exit times are hardly distinguishable; in case C, where $\mu(L_{3,2}) > \mu(L_{3,4})$, the statistics of north exit times are above those of south exit times, while the situation is reversed in case D where $\mu(L_{3,2}) \ll \mu(L_{3,4})$. The exponential fits on the figures have been drawn with a coefficient of proportionality equal to $\mu(L_{3,4})/\mu(L_{3,2})$.

In cases A and B, this ratio is equal to 1; in cases C and D the fits in figure 13 for the statistics are also proportional to the lobe areas, with very good agreement.

4.2.3 Escape from the jet

In figure 14 we show the amount of fluid, initially in R_3^* , that remains in R_3 as a function of dimensionless time, in cases A, B and C. The y -scale has been made dimensionless by dividing by $\mu(R_3^*)$. The calculations are performed by filling uniformly the two turnstile lobes $L_{2,3}$ and $L_{4,3}$ with points, and count how much points leave by the south or the north at each period, and then reconstruct the escape from R_3 using formula (41).

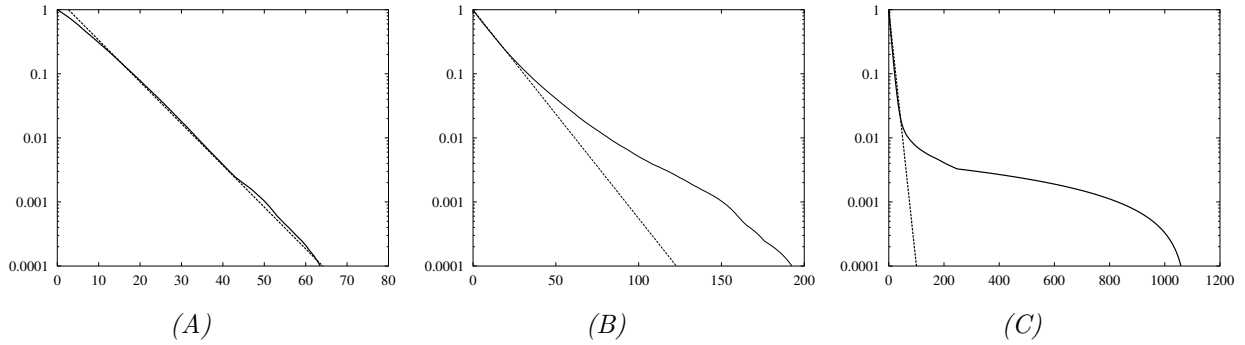


Figure 14: Amount of fluid, initially in R_3^* , still in R_3 as a function of dimensionless time, in cases A, B and C. In case B and C the decay is initially exponential, but departs from the exponential fit at larger times. The presence of regular islands inside R_3 , even if small, affects the dynamics of escape rate inside this region.

In cases A and D and in all the tests performed (even those not shown here), the decay rate inside the jet was found to be exponential whenever chaos was global in region R_3 ($R_3^* \equiv R_3$), like in the “Markov models” (see MacKay et al [1984], Meiss and Ott [1986]). In case B and C however, the decay rate is not exponential nor algebraic. It is interesting to note that in case C where the regular islands are very small, the decay is exponential up until 98% of the fluid initially in R_3^* has left region R_3 , but thereafter departs strongly from the exponential fit.

In region the northern region R_2 , we found algebraic decay in case A, but exponential decay in case B (not shown here); therefore it is very difficult to make assumptions on the *dynamics* of decay rate in a given region.

5 Towards a Good Estimate of Mean crossing Times Using Lobe Dynamics

Up to now we have presented results that could be obtained whether using a finite piece of manifolds ($\mu(L_{2,3})$, mean time spent in a region, ...) or else results that needed Monte-Carlo calculations (statistics of exit times, escape rate from a region, ...). $\mu(L^{n,s})$ was also calculated using the second method; however, $\mu(L^{n,s})$ is an infinite series which does not require the exact knowledge of the statistics of exit times (we just need to know how much fluid initially in $L_{2,3}$ finally exits by the south). Therefore, we could wonder whether it is possible to find a simpler way to estimate all the quantities of that type ($\mu(L^{n,s})$, $\mu(X^{n,s})$, ...). As seen in paragraph 3.4, three geometrical constraints expressed in the three equations (30), (31), and (29) already exist for the four unknowns $\mu(L^{n,s})$, $\mu(L^{n,n})$, $\mu(L^{s,n})$ and $\mu(L^{s,s})$; with one more relation we could estimate all those quantities.

5.1 The well-mixed hypothesis

In the preceding paragraph we have seen that we could write

$$\frac{\mu[f^j(L_{2,3}) \cap L_{3,2}]}{\mu(L_{3,2})} = \frac{\mu[f^j(L_{2,3}) \cap L_{3,4}]}{\mu(L_{3,4})} (1 + \varepsilon(j)), \quad (60)$$

where we expect $\varepsilon(j)$ to be small ($\varepsilon(j) \ll 1$) for j “sufficiently large.” Note that we do not make any assumption on how much fluid leaves at each iterate (as is done in the so-called “Markov models”, see MacKay et al [1984], Meiss and Ott [1986]). We just assume that the proportion of fluid that leaves from the north or the south on a given iteration is proportional to the area of the lobe through which it escapes. If we suppose that $\varepsilon(j) \approx 0$ for all j 's, we obtain a new relation and we can estimate all the unknown quantities.

5.1.1 Estimation of $\mu(L^{n,s})$, $\mu(L^{n,n})$, $\mu(L^{s,n})$ and $\mu(L^{s,s})$ using the well mixed hypothesis

When introducing assumption (60) in equation (15), we obtain the following equation:

$$\frac{\mu(L^{n,n})}{\mu(L_{3,2})} \approx \frac{\mu(L^{n,s})}{\mu(L_{3,4})}. \quad (61)$$

We obtain the following results:

$$\mu(L^{n,s}) \approx \frac{\mu(L_{4,3}) \mu(L_{2,3})}{\mu(L_{4,3}) + \mu(L_{2,3})} \quad (62)$$

$$\mu(L^{n,n}) \approx \frac{\mu(L_{2,3})^2}{\mu(L_{4,3}) + \mu(L_{2,3})} \quad (63)$$

$$\mu(L^{s,s}) \approx \frac{\mu(L_{4,3})^2}{\mu(L_{4,3}) + \mu(L_{2,3})} \quad (64)$$

$$\mu(L^{s,n}) = \mu(L^{n,s}). \quad (65)$$

5.1.2 Estimation of $\mu(X^{n,s})$, $\mu(X^{n,n})$, $\mu(X^{s,n})$ and $\mu(X^{s,s})$ using the well mixed hypothesis

Starting with eq. (60), multiplying by j and integrating using eq. (21), we obtain:

$$\frac{\mu(X^{n,n})}{\mu(L_{3,2})} \approx \frac{\mu(X^{n,s})}{\mu(L_{3,4})}. \quad (66)$$

We can also write an identical formula, starting from $L_{4,3}$ (fluid that comes from the south) instead of $L_{2,3}$ (fluid that comes from the north):

$$\frac{\mu(X^{s,n})}{\mu(L_{3,2})} \approx \frac{\mu(X^{s,s})}{\mu(L_{3,4})}. \quad (67)$$

This gives two more equations for the four unknowns $\mu(X^{n,s})$, $\mu(X^{n,n})$, $\mu(X^{s,n})$ and $\mu(X^{s,s})$, which, with the two geometrical constraints (32) and (33), allow us to solve the problem in an analogous manner as we solved for $\mu(L^{n,s})$, $\mu(L^{n,n})$, $\mu(L^{s,n})$ and $\mu(L^{s,s})$. We therefore obtain:

$$\begin{aligned}\mu(X^{n,n}) &\approx \frac{\mu^2(L_{2,3})}{[\mu(L_{4,3}) + \mu(L_{2,3})]^2} \mu(R_3^*) \\ \mu(X^{n,s}) &\approx \frac{\mu(L_{2,3}) \mu(L_{4,3})}{[\mu(L_{4,3}) + \mu(L_{2,3})]^2} \mu(R_3^*) \\ \mu(X^{s,s}) &\approx \frac{\mu^2(L_{4,3})}{[\mu(L_{4,3}) + \mu(L_{2,3})]^2} \mu(R_3^*) \\ \mu(X^{s,n}) &= \mu(X^{n,s}) .\end{aligned}\tag{68}$$

5.1.3 Estimation of Mean Crossing Times Using the Well Mixed Hypothesis

Using the results from above we obtain the mean crossing time:

$$\langle t^{n,s} \rangle \approx 1 + \frac{\mu(R_3^*)}{\mu(L_{4,3}) + \mu(L_{2,3})}\tag{69}$$

$$= 1 + \langle t_{R_3} \rangle ,\tag{70}$$

with a similar result for $\langle t^{n,n} \rangle$, $\langle t^{s,n} \rangle$ and $\langle t^{s,s} \rangle$. Although the numerical examples A, C and D show that these quantities all fall within 10% of $1 + \langle t_{R_3} \rangle$, the situation is quite different in case B. This implies that using this hypothesis, alone, is not sufficient to distinguish between the different crossing times. Therefore we need to take into account more details of Lobe Dynamics theory in order to improve those results.

5.2 Accuracy of Truncated Series of Lobe Intersections for the Statistical Quantities

The statistical quantities defined in equations (18) and (28) are expressed in terms of infinite series of areas of intersections of turnstile lobes. We showed before that the well-mixed hypothesis was not accurate enough to catch the differences between the different crossing times. Indeed, numerical results showed that this hypothesis failed for short times (small j in eq. (60)). However, for small j , it is quite easy to obtain those quantities directly using a finite piece of the stable and unstable manifolds, and calculating the area of intersections. Hence we can use the truncated series $\mu_{-}L^{n,s}(\ell)$ and $\mu_{-}X^{n,s}(\ell)$ defined in equations (42) and (56) respectively, and introduce the truncated series $\langle t^{n,s} \rangle(\ell)$ defined as:

$$\langle t^{n,s} \rangle(\ell) = 1 + \frac{\mu_{-}X^{n,s}(\ell)}{\mu_{-}L^{n,s}(\ell)}.\tag{71}$$

With these definitions, it is an easy calculation to show that as $\ell \rightarrow \infty$ we recover the exact series:

$$\begin{aligned}\lim_{\ell \rightarrow \infty} \mu_{-}L^{n,s}(\ell) &= \mu(L^{n,s}) \\ \lim_{\ell \rightarrow \infty} \mu_{-}X^{n,s}(\ell) &= \mu(X^{n,s}) \\ \lim_{\ell \rightarrow \infty} \langle t^{n,s} \rangle(\ell) &= \langle t^{n,s} \rangle.\end{aligned}$$

We can make the same definitions for the quantities associated with particles that enter the jet from from the north and exit to the north and, as above, we recover the exact series as $\ell \rightarrow \infty$.

One observes in examples that the area of the intersection of iterates of one turnstile lobe with another tends to get smaller as the iteration number gets larger. Therefore one might hope that a “small” (and practically computable) number of terms in the relevant series might lead to a reasonably accurate answer. We will now examine this question by considering numerical results for truncated series (using a finite piece of manifolds) and compare the results to “exact” results obtained through Monte Carlo simulation in case A. The area of the lobes and lobe intersections are calculated numerically as follows: their boundaries are

comprised of segments of stable and unstable manifolds, which are defined numerically by an ensemble of points. We first search for the intersection points of the curves, and then we can follow the pieces of stable and unstable manifolds between two intersection points. We therefore define the lobe intersections by a closed ensemble of points. Then it is just left to calculate the area by the trapezoidal rule.

ℓ	$\mu_{-}L^{n,s}(\ell)$	$\mu_{-}X^{n,s}(\ell)$	$\langle t^{n,s} \rangle(\ell)$	$\mu_{-}L^{n,n}(\ell)$	$\mu_{-}X^{n,n}(\ell)$	$\langle t^{n,n} \rangle(\ell)$
2	0.0666	0.1332	3.	0.	0.	--
3	0.0666	0.1332	3.	0.	0.	--
4	0.0666	0.1332	3.	0.0551	0.2204	5
5	0.0671	0.136	3.03	0.0705	0.2974	5.22
6	0.1403	0.5754	5.10	0.0764	0.3327	5.35
7	0.16	0.7135	5.46	0.112	0.5819	6.2
∞	0.356	3.78	11.6	0.345	4.01	12.6

Table 1: Statistics of north–south and north–north crossing for finite ℓ , in case A, calculated with formula 18 and 28, using a finite piece of manifolds; the infinite value was calculated numerically. The statistics given by the truncated series are still far from the infinite time value.

In table 1 we give values for different truncations (ℓ ranging from 2 to 7) of the different statistical quantities associated with north–south and the north–north crossing. As a consequence of the symmetry 9, they are, respectively, the same as the south–north and south–south crossing statistical quantities. The “exact answer,” i.e., infinite value of ℓ , was calculated numerically using the Monte-Carlo method. It is clear that even for $\ell = 8$, the average times calculated with truncated series are very different from the infinite (“exact”) value. Indeed, the geometrical constraints introduced in paragraph 3.4 are far from satisfied. This might lead one to believe that the formulae from lobe dynamics are of little practical value: exact computation of all the terms in these series would require a computation of the entire (infinite) length of the relevant stable and unstable manifolds. This is not possible.

5.3 From Truncated Series to Mixed Series: Accelerate Convergence for Lobe Dynamics

5.3.1 The fundamental hypothesis

Up to now, we have tried to estimate the infinite series defining $\mu(L^{n,s})$ and $\mu(X^{n,s})$ using two different methods:

1. *The well-mixed hypothesis* enables to evaluate roughly those quantities, but does not allow to distinguish the corresponding crossing times. Indeed, this hypothesis fails for short time exits (small j in equation 60)
2. *The truncated series* fail in the evaluation of the infinite series, since all terms for moderate up to large j are taken equal to zero; however the results for short time exit are accurate.

It is therefore natural to introduce *accelerate series* that mix the two methods:

1. For small js the terms in the series are calculated using the area of intersections of lobes (truncated series).
2. For moderate up to large js we suppose that the well-mixed hypothesis holds.

We begin by writing an expression for the remainder of the series defining $\mu(L^{n,s})$ and $\mu(L^{n,n})$. These are given by:

$$\begin{aligned}\Delta\mu_{-}L^{n,s}(\ell) &= \mu(L^{n,s}) - \mu_{-}L^{n,s}(\ell) \\ &= \sum_{j=\ell+1}^{\infty} \mu[f^j(L_{2,3}) \cap L_{3,4}] .\end{aligned}\quad (72)$$

and

$$\begin{aligned}\Delta\mu_{-}L^{n,n}(\ell) &= \mu(L^{n,n}) - \mu_{-}L^{n,n}(\ell) \\ &= \sum_{j=\ell+1}^{\infty} \mu[f^j(L_{2,3}) \cap L_{3,2}] .\end{aligned}\quad (73)$$

Rather than using eq. (60), it is more convenient to use an integrated form :

$$\frac{\sum_{j=\ell+1}^{\infty} \mu[f^j(L_{2,3}) \cap L_{3,2}]}{\mu(L_{3,2})} = \frac{\sum_{j=\ell+1}^{\infty} \mu[f^j(L_{2,3}) \cap L_{3,4}]}{\mu(L_{3,4})} + \sum_{j=\ell+1}^{\infty} \varepsilon(j) \frac{\mu[f^j(L_{2,3}) \cap L_{3,4}]}{\mu(L_{3,4})} \quad (74)$$

or

$$\frac{\mu(L^{n,n}) - \mu_{-}L^{n,n}(\ell)}{\mu(L_{3,2})} = \frac{\mu(L^{n,s}) - \mu_{-}L^{n,s}(\ell)}{\mu(L_{3,4})} + \varepsilon_L(\ell) , \quad (75)$$

where

$$\varepsilon_L(\ell) \equiv \sum_{j=\ell+1}^{\infty} \varepsilon(j) \frac{\mu[f^j(L_{2,3}) \cap L_{3,4}]}{\mu(L_{3,4})} . \quad (76)$$

Note that, if, as we expect, $\varepsilon_L(\ell)$ is small, than equation 75 says physically that *The quantity of fluid from the turnstile lobe $L_{2,3}$ still in R_3 after ℓ iterates, and which will escape by the south or by the north is proportional to the area of the lobe through which it escapes.*

5.3.2 Construction of Mixed Series with Accelerated Convergence

Using the assumption embodied in eq. (75), as well as the three geometrical constraints expressed in the three equations (30), (31), and (29), we now have four independent (linear) equations that we can solve for the four unknowns $\mu(L^{n,s})$, $\mu(L^{n,n})$, $\mu(L^{s,n})$ and $\mu(L^{s,s})$. Doing this gives:

$$\mu(L^{n,s}) = \mu_{-}L^{n,s}(\ell) + \beta [\mu(L_{2,3}) - \mu_{-}L^{n,s}(\ell) - \mu_{-}L^{n,n}(\ell)] - \varepsilon_L(\ell) \beta \mu(L_{2,3}) \quad (77)$$

$$\mu(L^{n,n}) = \mu_{-}L^{n,n}(\ell) + (1 - \beta) [\mu(L_{2,3}) - \mu_{-}L^{n,s}(\ell) - \mu_{-}L^{n,n}(\ell)] + \varepsilon_L(\ell) \beta \mu(L_{2,3}) \quad (78)$$

$$\mu(L^{s,n}) = \mu(L^{n,s}) \quad (79)$$

$$\mu(L^{s,s}) = \mu(L_{4,3}) - \mu(L^{s,n}) , \quad (80)$$

where

$$\beta = \frac{\mu(L_{3,4})}{\mu(L_{2,3}) + \mu(L_{3,4})} . \quad (81)$$

Therefore, we define mixed series with accelerated convergence as follows:

$$\begin{aligned}\mu_{-}L_{acc}^{n,s}(\ell) &= \mu_{-}L^{n,s}(\ell) + \beta [\mu(L_{2,3}) - \mu_{-}L^{n,s}(\ell) - \mu_{-}L^{n,n}(\ell)] \\ \mu_{-}L_{acc}^{n,n}(\ell) &= \mu_{-}L^{n,n}(\ell) + (1 - \beta) [\mu(L_{2,3}) - \mu_{-}L^{n,s}(\ell) - \mu_{-}L^{n,n}(\ell)] \\ \mu_{-}L_{acc}^{s,n}(\ell) &= \mu_{-}L_{acc}^{n,s}(\ell) \\ \mu_{-}L_{acc}^{s,s}(\ell) &= \mu(L_{4,3}) - \mu_{-}L_{acc}^{s,n}(\ell) .\end{aligned}\quad (82)$$

We have the following fundamental equation giving the difference between the corrected series and the exact series:

$$\mu(L^{n,s}) = \mu_{-}L_{acc}^{n,s}(\ell) + \varepsilon_L(\ell) \beta \mu(L_{2,3}) . \quad (83)$$

5.3.3 Properties of the Series with Accelerated Convergence

The mixed series have several desirable properties that we collect here.

- *The mixed series converge towards the same limit as the truncated series.*

Proof: By examining eq. (75), one can check that $\varepsilon_L(\ell)$ is equal to the difference of two positive terms, each of which goes to zero as ℓ goes to infinity. Therefore

$$\lim_{\ell \rightarrow \infty} \varepsilon_L(\ell) = 0 , \quad (84)$$

so that, from eq. (83),

$$\lim_{\ell \rightarrow \infty} \mu_{-L_{acc}^{n,s}}(\ell) = \mu(L^{n,s}) . \quad (85)$$

□

- *If all $\varepsilon(j)$ s in equation 60 are small for $j \geq \ell + 1$, then $\varepsilon_L(\ell)$ is also small.*

Proof: Let

$$\varepsilon_0 = \sup_{j \geq \ell + 1} |\varepsilon(j)| . \quad (86)$$

Then $\varepsilon_0 \ll 1$ and

$$|\varepsilon_L(\ell)| \leq \varepsilon_0 \sum_{j=\ell+1}^{\infty} \frac{\mu[f^j(L_{2,3}) \cap L_{3,4}]}{\mu(L_{3,4})} \quad (87)$$

$$\leq \varepsilon_0 \frac{\mu(L^{n,s}) - \mu_{-L^{n,s}}(\ell)}{\mu(L_{3,4})} . \quad (88)$$

□

If $\varepsilon_L(\ell)$ is small then the mixed series converge much more rapidly than the truncated series. In that case the correction in equation (83) is such that

$$\varepsilon_L(\ell) \leq \varepsilon_0 \frac{\mu(L_{2,3})}{\mu(L_{2,3}) + \mu(L_{3,4})} (\mu(L^{n,s}) - \mu_{-L^{n,s}}(\ell)) , \quad (89)$$

which proves that the correction is indeed negligible.

5.3.4 Construction of Mixed Series for $\mu(X^{n,s})$, $\mu(X^{n,n})$, $\mu(X^{s,n})$ and $\mu(X^{s,s})$.

Starting with eq. (60), we have

$$\frac{j \mu[f^j(L_{2,3}) \cap L_{3,2}]}{\mu(L_{3,2})} = \frac{j \mu[f^j(L_{2,3}) \cap L_{3,4}]}{\mu(L_{3,4})} (1 + \varepsilon(j)) , \quad (90)$$

from which it follows that:

$$\frac{\mu(X^{n,n}) - \mu_{-X^{n,n}}(\ell)}{\mu(L_{3,2})} = \frac{\mu(X^{n,s}) - \mu_{-X^{n,s}}(\ell)}{\mu(L_{3,4})} + \varepsilon_X(\ell) , \quad (91)$$

with

$$\varepsilon_X(\ell) = \sum_{j=\ell+1}^{\infty} \frac{j \varepsilon(j) \mu[f^j(L_{2,3}) \cap L_{3,4}]}{\mu(L_{3,4})} . \quad (92)$$

We can also write an identical formula, starting from $L_{4,3}$ (fluid that comes from the south) instead of $L_{2,3}$ (fluid that comes from the north):

$$\frac{\mu(X^{s,s}) - \mu_{\neg} X^{s,s}(\ell)}{\mu(L_{3,4})} = \frac{\mu(X^{s,n}) - \mu_{\neg} X^{s,n}(\ell)}{\mu(L_{3,2})} + \varepsilon'_X(\ell), \quad (93)$$

with

$$\varepsilon'_X(\ell) = \sum_{j=\ell+1}^{\infty} \frac{j \varepsilon(j) \mu[f^j(L_{4,3}) \cap L_{3,2}]}{\mu(L_{3,2})}. \quad (94)$$

This gives two more equations for the four unknowns $\mu(X^{n,s})$, $\mu(X^{n,n})$, $\mu(X^{s,n})$ and $\mu(X^{s,s})$, which, with the two geometrical constraints (32) and (33), allow us to solve the problem in an analogous manner as we solved for $\mu(L^{n,s})$, $\mu(L^{n,n})$, $\mu(L^{s,n})$ and $\mu(L^{s,s})$. We therefore obtain the mixed series with accelerated convergence:

$$\begin{aligned} \mu_{\neg} X_{acc}^{n,n}(\ell) &= (1-\beta)^2 \text{rem}_{R_3^*}(\ell) + \mu_{\neg} X^{n,n}(\ell) - (1-\beta) \mu_{\neg} X^{n,s}(\ell) + (1-\beta) \mu_{\neg} X^{s,n}(\ell) \\ \mu_{\neg} X_{acc}^{n,s}(\ell) &= \beta(1-\beta) \text{rem}_{R_3^*}(\ell) + (1-\beta) \mu_{\neg} X^{n,s}(\ell) + \beta \mu_{\neg} X^{s,n}(\ell) \\ \mu_{\neg} X_{acc}^{s,n}(\ell) &= \beta(1-\beta) \text{rem}_{R_3^*}(\ell) + (1-\beta) \mu_{\neg} X^{n,s}(\ell) + \beta \mu_{\neg} X^{s,n}(\ell) \\ \mu_{\neg} X_{acc}^{s,s}(\ell) &= \beta^2 \text{rem}_{R_3^*}(\ell) + \mu_{\neg} X^{s,s}(\ell) + \beta \mu_{\neg} X^{n,s}(\ell) - \beta \mu_{\neg} X^{s,n}(\ell), \end{aligned} \quad (95)$$

where $\text{rem}_{R_3^*}(\ell)$ stands for

$$\text{rem}_{R_3^*}(\ell) = \mu(R_3^*) - \mu_{\neg} X^{n,n}(\ell) - \mu_{\neg} X^{n,s}(\ell) - \mu_{\neg} X^{s,n}(\ell) - \mu_{\neg} X^{s,s}(\ell). \quad (96)$$

Using the same reasoning as above, one can prove that the corrected series converge towards the same limit as the truncated series, but more rapidly.

5.3.5 Mixed Series for Mean Crossing Time

Using the results from above we obtain mixed series for the mean crossing times at step ℓ :

$$\langle t^{n,s} \rangle_{acc}(\ell) = 1 + \frac{\mu_{\neg} X_{acc}^{n,s}(\ell)}{\mu_{\neg} L_{acc}^{n,s}(\ell)} \quad (97)$$

$$\langle t^{n,n} \rangle_{acc}(\ell) = 1 + \frac{\mu_{\neg} X_{acc}^{n,n}(\ell)}{\mu_{\neg} L_{acc}^{n,n}(\ell)}, \quad (98)$$

with similar formula for $\langle t^{s,n} \rangle_{acc}(\ell)$ and $\langle t^{s,s} \rangle_{acc}(\ell)$.

Finally, we emphasize once again that the assumptions we have made are completely geometric. They do not require any dynamical assumptions as, for example, in the Markov model approach of MacKay et al. [1984] and Meiss and Ott [1986]. In particular, we make no assumptions such as exponential or algebraic decay, or on *how much fluid* goes in or out of a given region at each iterate ℓ .

5.4 Numerical results

We now apply our formula for accelerated convergence of series to the numerical simulations of transport in the meandering jet presented in section 4. It should be emphasized that the mixed series require computation only with pieces of the manifolds of finite length, i.e. finite ℓ .

5.4.1 Case A: Full North-South Symmetry with $R_3^* \approx R_3$

For our example, since $R_3^* \approx R_3$, $\beta = 1/2$, $\mu(L^{n,n}) = \mu(L^{s,s})$, $\mu(X^{n,n}) = \mu(X^{s,s})$, we obtain, using eqs. (82) and (95):

$$\mu_{\neg} L_{acc}^{n,s}(\ell) = \frac{\mu(L_{2,3}) + \mu_{\neg} L^{n,s}(\ell) - \mu_{\neg} L^{n,n}(\ell)}{2} \quad (99)$$

$$\mu_{\neg} L_{acc}^{n,n}(\ell) = \frac{\mu(L_{2,3}) - \mu_{\neg} L^{n,s}(\ell) + \mu_{\neg} L^{n,n}(\ell)}{2} \quad (100)$$

$$\mu_{-X_{acc}^{n,s}}(\ell) = \frac{\mu(R_3) + 2\mu_{-X^{n,s}}(\ell) - 2\mu_{-X^{n,n}}(\ell)}{4} \quad (101)$$

$$\mu_{-X_{acc}^{n,n}}(\ell) = \frac{\mu(R_3) + 2\mu_{-X^{n,n}}(\ell) - 2\mu_{-X^{n,s}}(\ell)}{4}. \quad (102)$$

All the results are shown in table 2: once again, we emphasize that only geometrical assumptions have been made. In this case we found that the first connection between manifolds associated with the northern and

ℓ	$\mu_{-L_{acc}^{n,s}}(\ell)$	$\mu_{-X_{acc}^{n,s}}(\ell)$	$\langle t^{n,s} \rangle_{acc}(\ell)$	$\mu_{-L_{acc}^{n,n}}(\ell)$	$\mu_{-X_{acc}^{n,n}}(\ell)$	$\langle t^{n,n} \rangle_{acc}(\ell)$
2	0.3838	3.97	11.3	0.3172	3.83	13.1
3	0.3838	3.97	11.3	0.3172	3.83	13.1
4	0.356	3.86	11.8	0.345	3.94	12.4
5	0.349	3.82	11.9	0.352	3.98	12.3
6	0.382	4.02	11.5	0.319	3.78	12.8
7	0.374	3.97	11.6	0.327	3.83	12.7
∞	0.356	3.78	11.6	0.345	4.01	12.6

Table 2: Estimated statistics of north–south and north–north crossing for finite ℓ . Those finite time statistics agree extremely well with the infinite value calculated numerically, even for ℓ small. $\ell = \infty$ represents the “exact” value obtained by Monte Carlo calculation.

southern boundaries of the jet occurs for $\ell = 2$, while the first connection between manifolds governing transport from north to north occurs for $\ell = 4$. It is interesting to note that the corrected series are already quite well converged for $\ell = 4$.

5.5 Case B: Full North-South Symmetry with $R_3^* \not\approx R_3$

First, let us consider a first approximation that $\mu(R_3^*) = \mu(R_3)$. With this (inaccurate) approximation we obtain the following results for the mixed series: We might wonder whether the slight difference between

ℓ	$\mu_{-L_{acc}^{n,s}}(\ell)$	$\mu_{-X_{acc}^{n,s}}(\ell)$	$\langle t^{n,s} \rangle_{acc}(\ell)$	$\mu_{-L_{acc}^{n,n}}(\ell)$	$\mu_{-X_{acc}^{n,n}}(\ell)$	$\langle t^{n,n} \rangle_{acc}(\ell)$
2	0.372	5.94	17.0	0.61	6.27	11.3
3	0.366	5.93	17.2	0.615	6.29	11.2
4	0.352	5.87	17.7	0.63	6.35	11.1
7	0.354	5.86	17.6	0.628	6.35	11.1
∞	0.356	5.51	16.5	0.626	5.945	10.5

Table 3: Estimated statistics of north–south and north–north crossing for finite ℓ . Here we have taken $\mu(R_3^*) = \mu(R_3)$, which is not exact. Therefore the results, already converged for $\ell = 2$, are slightly overestimated. The values for $\ell = \infty$ were calculated numerically with a Monte-Carlo method, like before.

the results obtained here for the mixed series and the numerical values is only due to the overestimation of $\mu(R_3^*)$ that results from taking $\mu(R_3^*) = \mu(R_3)$. In order to answer this, we now show the same table, but

ℓ	$\mu_{-}L_{acc}^{n,s}(\ell)$	$\mu_{-}X_{acc}^{n,s}(\ell)$	$\langle t^{n,s} \rangle_{acc}(\ell)$	$\mu_{-}L_{acc}^{n,n}(\ell)$	$\mu_{-}X_{acc}^{n,n}(\ell)$	$\langle t^{n,n} \rangle_{acc}(\ell)$
2	0.372	5.56	15.9	0.61	5.89	10.7
3	0.366	5.55	16.1	0.615	5.91	10.6
4	0.352	5.49	16.6	0.63	5.97	10.5
7	0.354	5.48	16.5	0.63	5.97	10.5
∞	0.356	5.51	16.5	0.626	5.945	10.5

Table 4: Estimated statistics of north–south and north–north crossing for finite ℓ . Here we have taken the real value for $\mu(R_3^*)$, calculated numerically. The results are now completely converged.

where the real value of the chaotic region, $\mu(R_3^*) = 22.9$, calculated numerically, was used. Here, the first connection of manifolds leading to transport across the jet between north and south occurs for $\ell = 3$, while the first connection between manifolds leading to transport between north and north occurs for $\ell = 1$. Once again, the results are well converged for the first value where both north-south and north-north connections have occurred ($\ell = 3$).

5.5.1 Case C: No South-North Symmetry, $\mu(R_3^*) \approx \mu(R_3)$

We give the tables for the mixed series of north–south, north–north, south–north and south–south crossing statistics. In this case we considered that $\mu(R_3^*) \approx \mu(R_3)$. Once again, one can see very good agreement between the finite-time statistics and the infinite values calculated numerically (Monte-Carlo method). In

ℓ	$\mu_{-}L_{acc}^{n,s}(\ell)$	$\mu_{-}X_{acc}^{n,s}(\ell)$	$\langle t^{n,s} \rangle_{acc}(\ell)$	$\mu_{-}X_{acc}^{n,n}(\ell)$	$\langle t^{n,n} \rangle_{acc}(\ell)$	$\mu_{-}X_{acc}^{s,s}(\ell)$	$\langle t^{s,s} \rangle_{acc}(\ell)$
1	0.656	6.16	10.4	8.7	9.49	4.49	9.17
2	0.642	6.12	10.5	8.86	9.53	4.41	8.83
3	0.705	6.31	9.95	8.64	9.86	4.24	9.49
7	0.71	6.35	9.9	8.5	9.8	4.29	9.8
∞	0.69	6.23	10.0	8.2	9.3	4.9	10.7

Table 5: Mixed series for the case $c = 0.1$, $\omega = 0.5$, $\epsilon_1 = 0.45$ and $\epsilon_2 = 0.2$ for small ℓ . Although the flow is not symmetric with respect to north-south transport, and vice versa, the results are quite good even for such a small ℓ as $\ell = 3$.

this case the first intersection between manifolds giving rise to north-south transport occurs for $\ell = 2$, while the first intersection between manifolds giving rise to north-north transport occurs for $\ell = 1$, and the first connection between manifolds giving rise to south-south transport occurs for $\ell = 1$. Although in this case the results converge much less rapidly, they are reasonably converged for $\ell = 2$. We searched for the value of β for which the convergence was the most rapid and found that if we took $\beta = 0.44$, the corrected series were completely converged for $\ell = 4$ (here $\beta = 0.418$, that is, not very far from this value).

5.5.2 Case D: very asymmetric with $\mu(R_3^*) \approx \mu(R_3)$

In this very asymmetric case we obtained the following results for the mixed series: Once again, the results are quite good (especially if we consider that the mean time is the ratio of two estimated quantities). In this

ℓ	$\mu-L_{acc}^{n,s}(\ell)$	$\mu-X_{acc}^{n,s}(\ell)$	$\langle t^{n,s} \rangle_{acc}(\ell)$	$\mu-X_{acc}^{n,n}(\ell)$	$\langle t^{n,n} \rangle_{acc}(\ell)$	$\mu-X_{acc}^{s,s}(\ell)$	$\langle t^{s,s} \rangle_{acc}(\ell)$
1	0.247	3.02	13.2	1.13	13.2	8.06	13.2
2	0.253	3.032	13.0	1.13	13.9	8.04	13.3
3	0.253	3.032	13.0	1.13	13.9	8.04	13.3
4	0.220	2.87	14.0	1.16	10.7	8.32	13.1
7	0.228	2.95	13.9	1.26	12.2	8.06	12.9
∞	0.217	2.88	14.3	1.3	11.9	8.12	12.9

Table 6: Mixed series for the case $c = 0.2$, $\omega = 0.85$, $\epsilon_1 = 0.9$ and $\epsilon_2 = 0.15$ for finite ℓ . Although the flow is not symmetric, the results are quite good even for such a small ℓ as $\ell = 3$.

case the first intersection between manifolds leading to north-south transport occurs for $\ell = 2$, while the first intersection between manifolds leading to north-north transport occurs for $\ell = 4$, and the first intersection between manifolds leading to south-south connection occurs for $\ell = 4$. Once again, the results are reasonably converged for $\ell = 4$, and are almost exact for $\ell = 7$.

6 Summary

We have shown that lobe dynamics forms the essential spatio-temporal mechanism for transport associated with a meandering jet subject to periodic variability. Using the framework of lobe dynamics we have shown how to compute:

- the mean passage time across the jet,
- the mean residence time in the jet, and
- the location, and area, of the set of points that cross the jet.

Each of these quantities is expressed in terms of an infinite series of areas of intersections of turnstile lobes. As such, they are not practically computable. In order to deal with this problem we develop “mixed series” that exhibit an accelerated convergence in the sense that a low order truncation, equivalently, “relatively short” pieces of manifolds of finite length, gives a very accurate approximation to the sum of the series. We demonstrate this through numerical simulation of the jet for a variety of parameter values illustrating different flow regimes.

Finally, we remark that our results are much more broadly applicable. For example, the meandering jet has the same geometrical features as the forced pendulum.

References

- Boffetta, G., Lacorata, G., Redaelli, G., Vulpiani, A. [2001] Detecting barriers to transport: a review of different techniques. *Physica D*, **159**, 58-70.
- Bower, A. S. [1991] A simple kinematic mechanism for mixing fluid parcels across a meandering jet. *J. Phys. Oceanogr.*, **21**, 173-180.
- del-Castillo-Negrete, D. [1998] Asymmetric transport and non-Gaussian statistics of passive scalars in vortices in shear *Physics of Fluids*, **10** (3), 576-594.
- Duan, J., Wiggins, S. [1996] Fluid Exchange Across a Meandering Jet with Quasiperiodic Variability. *Journal of Physical Oceanography*, **26**(7), 1176-1180.
- MacKay, R. S., Meiss, J. D., Percival, I. C. [1984] Transport in Hamiltonian systems. *Physica D*, **13**(1-2), 55-81.
- Meiss, J. D., Ott, E. [1986] Markov tree model of transport in area-preserving maps. *Physica D*, **20**(2-3), 387-402.
- Meiss, J. D. [1997] Average exit time for volume-preserving maps. *Chaos*, **7**(1), 139-147.
- Poje, A. C., Haller, G. [1999] Geometry of cross-stream mixing in a double-gyre ocean model. *J. Phys. Oceanogr.*, **29**, 1649-1665.
- Rogerson, A., Miller, P. D., Pratt, L., Jones, C. K. R. T. [1999] Lagrangian motion and fluid exchange in a barotropic meandering jet. *J. Phys. Oceanogr.*, **29**, 2635-2655.
- Rom-Kedar, V., Wiggins, S. [1990] Transport in Two Dimensional Maps *Archive for Rational Mechanics and Analysis*, **109**(3), 239-298.
- Rom-Kedar, V. [1994] Homoclinic tangles-classification and applications. *Nonlinearity*, **7**, 441-473.
- Samelson, R. M. [1992] Fluid exchange across a meandering jet. *J. Phys. Oceanogr.*, **22**(4), 431-440.
- Wiggins, S. [1992] *Chaotic Transport in Dynamical Systems*. Springer-Verlag: New York.
- Wiggins, S. [2005] The dynamical systems approach to Lagrangian transport in oceanic flows. *Annu. Rev. Fluid Mech.*, **37**, 295-328.
- Yuan, G.-C., Pratt, L. J., Jones, C. K. R. T. [2002] Barrier destruction and Lagrangian predictability at depth in a meandering jet. *Dyn. Atmos. Oceans*, **35**, 41-61.